INSTRUMENTATION TO DETERMINE THE PRESENCE AND ACOUSTIC EFFECT OF MICROBUBBLES NEAR THE SEA SURFACE

PAT D. BARNHOUSE
MICHAEL J. STOFFEL
ROBERT E. ZIMDAR

MONT 30

INSTRUMENTATION TO DETERMINE THE PRESENCE AND ACOUSTIC EFFECT OF MICROBUBBLES NEAR THE SEA SURFACE

* * * * * *

Pat D. C. Barnhouse

Michael J. Stoffel

Robert E. Zimdar

INSTRUMENTATION TO DETERMINE THE PRESENCE AND ACOUSTIC EFFECT OF MICROBUBBLES NEAR THE SEA SURFACE

by

Pat D. C. Barnhouse

Lieutenant Commander, Royal Canadian Navy

Michael J. Stoffel

Lieutenant Commander, United States Navy

Robert E. Zimdar

Lieutenant, United States Navy

Submitted in partial fulfillment of
the requirements for the degree of

MASTER OF SCIENCE
IN
ENGINEERING ELECTRONICS

United States Naval Postgraduate School
Monterey, California

1 9 6 4

INSTRUMENTATION TO DETERMINE THE PRESENCE AND ACOUSTIC EFFECT OF MICROBUBBLES NEAR THE SEA SURFACE

by

Pat D. C. Barnhouse

Michael J. Stoffel

Robert E. Zimdar

This work is accepted as fulfilling

the thesis requirements for the degree of

MASTER OF SCIENCE

IN

ENGINEERING ELECTRONICS

from the

United States Naval Postgraduate School

ABSTRACT

The acoustic effects of air bubbles in water have been the subject of much investigation and speculation since the early days of World War II. Preliminary investigations have indicated the probable presence of microbubbles in varying concentrations in the body of the ocean, but their distribution and effect has not been the subject of definitive measurement. The construction and evaluation of equipment for "in situ" measurement of bubble size and distribution, and bubble-caused sound attenuation is discussed. The determination of bubble size and distribution by photographic means is described, and the superiority of a pulse technique in obtaining sound attenuation is demonstrated.

ACKNOWLEDGEMENTS

The writers wish to express their appreciation to Professor Herman Medwin of the Physics Department, U. S. Naval Postgraduate School, Monterey, California, for his guidance and encouragement of the experimental work, to Mr. Robert Moeller and Mr. Harold Whitfill of the Physics Department for their help in construction and acquisition of equipment, and to Dr. James A Mattison of Salinas for his guidance in developing methods of underwater photography. Thanks are also due to the U. S. Navy Underwater Sound Reference Laboratory for providing the EDO 327 transducer. This work was supported in part by the Office of Naval Research.

TABLE OF CONTENTS

LIST OF ILLUSTRATIONS

I

INTRODUCTION

The acoustic effects of air bubbles in water have been the subject of a great deal of investigation during and since World War II[8]. To varying degrees, depending on size and distribution, the presence of bubbles in water may have a marked effect on the absorption, scattering, and velocity of sound in water[8,10,17-19,23,28,29]. In addition, theories have recently been advanced that suggest that bubbles may have a great effect on meterological conditions at sea[7].

Up to now the existance of bubbles in sea water under most conditions has been largely a matter of speculation. The existance of bubbles in sea water in many specific locales or situations such as surf, wakes, and heavy seas is obvious. However, their existance under more normal conditions or in open sea has not been definitely established, although their presence has been frequently assumed in order to help explain certain observed effects, e.g. "surface reverberation[15,29]." Experiments recently conducted suggest that bubbles most likely to persist are of radius 30 to 120 microns (1 micron = 10^{-6} meter)[14].

Primarily because of the effect of wakes on sonar detection, a considerable body of theory concerning the effect of air bubbles on sound propagation in the sea has evolved[8,11,18,19,28,29]. Many attempts at verification of the various aspects of bubble theory have been made under laboratory conditions, but virtually none at sea.

In the hope that some of the uncertainty in this area might be dispelled, the project to determine the actual bubble distribution in sea water was undertaken. To accomplish this goal, the following objectives were set:

1. The design and test of equipment to determine the attenuation of sound in sea water over a frequency range of 20 to 200 kcs, to a depth of 50 feet.

2. The determination of air bubble distribution in sea water to depths of 50 feet.

The achievement of these goals required the development of a broad-band, sensitive method of measuring attenuation as a function of frequency. Two systems of measurement were studied: an acoustic impedance (interferometer) technique using a commercial transducer in a continuous-wave mode, and a pulse technique which required the construction of a large electrostatic transducer. The pulsed system using this transducer was expected to offer the following advantages over the interferometer method:

1. A flat output over a wide frequency range, and sharp pulse characteristics.

2. A method of determining velocity.

At the beginning of the project nothing was known about the distribution of a bubble size and their density in sea water. Therefore, even though the measurement of attenuation and, hopefully, bubble distribution could be accomplished by acoustic means, it was decided to develop a method of photographing bubbles is situ. Such photographs would provide a positive indication of the presence

of bubbles and furnish an alternative method of determining bubble density.

What follows in Parts II and III is a detailed discussion of the two attenuation measurement techniques developed. In part IV the design and test of bubble photography techniques and equipment is described.

II

ACOUSTIC TRANSMISSION LINE (INTERFEROMETER) METHOD

A. General

The acoustic transmission line method of measuring the acoustic properties of fluids and absorptive materials has been discussed by several authors [2,4,6,9] since the original paper by J. C. Hubbard.[1] Usually this apparatus consists of a plane transducer and parallel reflector in which standing plane waves are set up and measurements of impedence are made over a range of frequencies at one position, or in various positions at one frequency. Generally this method has been applied in an enclosed system and thus was considered unsuitable for the investigations discussed here. What was needed was a method that allowed for "in situ" attenuation measurements without disturbing the medium under investigation. This consideration gave rise to the design of an open system employing a transducer and reflector that could be immersed in sea water without causing any disturbance of that medium. Styrofoam was chosen as the reflector since this material has a ρc much less than the ρc of water, and therefore has excellent reflective properties for acoustic waves in water. The transducer used was an $8\frac{1}{2}$ inch, Edo 327 ADP mosaic "piston-type" transducer provided by USNUSRL. A general description of this transducer is given in Appendix II, 1.

[1]Hubbard, J. C. The acoustic resonator interferometer: I. The acoustic system and its equivalent electric network, Physical Review, v. 38, Sep., 1931: 1011-1019

B. Transducer Characteristics

The motional admittance circle near resonance method was used to obtain the characteristics of the transducer [1,4,5,6]. The equivalent electrical circuit of a piezoelectric transducer can be drawn as shown in Figure II, 1. If the components of the input admittance Y_I, this is, the input conductance (G_p) and input susceptance (C_p) of the transducer are measured over a range of frequencies (centered around the resonance frequency of the transducer) while radiating into an infinite field, and then conductance is plotted against the motional component of susceptance, a motional admittance circle such as is shown in Figure II, 2 is obtained. Since the radiation loading in air and water is very different, the diameter of the circles in both cases will be different. Compared with the effect in water a transducer will be unloaded in air, and so from the motional admittance circles the following results can be obtained:

$$R_M = \frac{1}{D_A}$$

$$R_R + R_M = \frac{1}{D_W}$$

$$R_o = \frac{1}{G_E}$$

Also, C_o can be found from the susceptance at the resonant frequency, because at this frequency there is no net contribution from L and C. Then

$$C = C_o\left[\left(\frac{f_a}{f_r}\right)^2 - 1\right]$$

$$L = \frac{1}{(2\pi f_r)^2 C}$$

Where f_r is the resonant frequency and f_a is the anti-resonant frequency.

CRYSTAL TRANSDUCER EQUIVALENT ELECTRICAL CIRCUIT

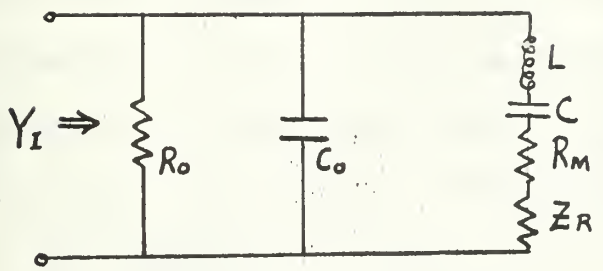

Y_I = INPUT ADMITTANCE
R_o = LEAKAGE RESISTANCE
C_o = BLOCKED CAPACITANCE
L = MOTIONAL INDUCTANCE
C = MOTIONAL CAPACITANCE
R_M = MOTIONAL RESISTANCE
$Z_R = R_R + jX_R$ = RADIATION IMPEDANCE
$Y_I = G_p + j\omega C_p$
$R = R_R + R_M$
$X_R = 0$ IN FREE FIELD (Ka high)

FIGURE II, 1

MOTIONAL ADMITTANCE CIRCLES

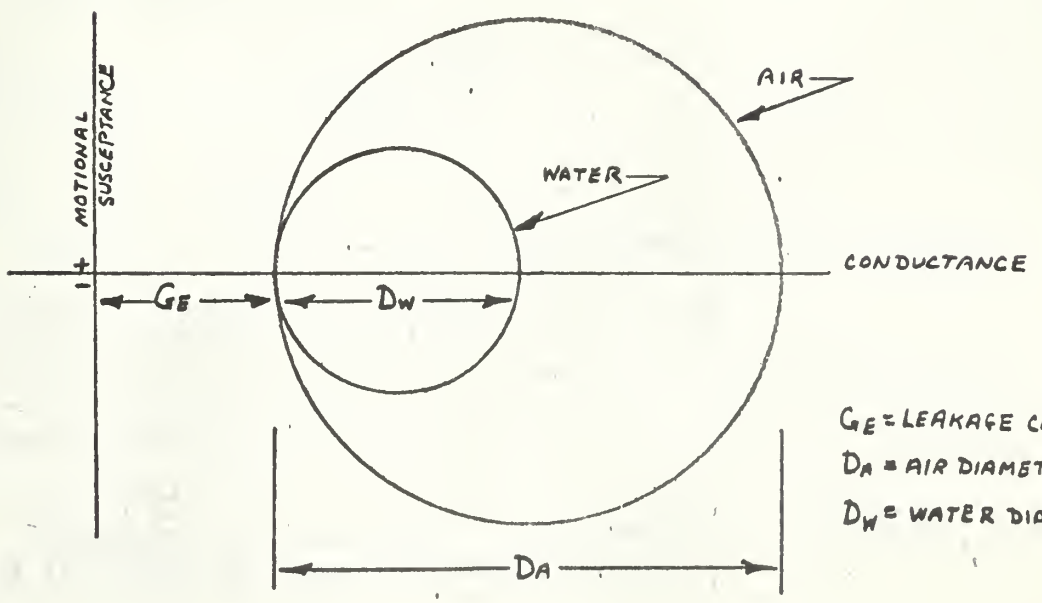

G_E = LEAKAGE CONDUCTANCE
D_A = AIR DIAMETER (MHOS)
D_W = WATER DIAMETER (MHOS)

FIGURE II, 2

For the Edo 327 this procedure had to be modified since it was discovered that this particular transducer was not effectively unloaded when radiating into air (i.e. the motional admittance circle in air was comparable in size to that in water). This was undoubtedly a consequence of the oil-filled diaphragm that covered the ADP crystals. From the motional admittance circle measurements R_o, $(R_R + R_M)$, C_o, C and L can be found. It is also known that near resonance[2]

$$\frac{C}{L} = \frac{8\phi^2 S_{22} \ell_y}{\pi^2 S_y} \cdot \frac{2\phi^2}{\rho \ell_y S_y}$$

Where ϕ = electro mechanical transformation factor

S_{22} = compliance coefficient of transducer crystal

ℓ_y = y dimension of transducer crystal

S_y = cross sectional area perperdicular to y axis. (Effective piston cross sectional area in this case)

ρ = density of crystal material

and all units are mks

Therefore $$\frac{\phi^2}{S_y} = \left(\frac{C\pi^2 \rho}{16 L S_{22}} \right)^{1/2}$$

Also $$R_R = \rho_o c_o \frac{S_y}{\phi^2}$$

Where $\rho_o c_o$ = specific acoustic impedance of water (in rayls)

Now the following can be evaluated: R_R, R_M, ϕ^2

For use in the experimental work described here the quantities in electrical units have to be transformed into units of mechanical

[2]Kinsler, L. E. and Frey, A. R. Fundamentals of Acoustics, 2nd Ed. Wiley and Sons, Inc., 1962: 337-343

impedance. For example, the radiation resistance for the infinite field, $R_r = \phi^2 R_R$ in mechanical units. Calculated characteristics for the Edo 327 transucer are given in Appendix II, 2.

C. Systemization of Equations

In the experimental work, measurements were made of the input conductance and susceptance of the transducer over a desired range of frequencies (as will be discussed more fully in a later section). However, the radiation impedance of the transducer was desired for subsequent calculations of bubble attenuation. This section indicates how these desired values were obtained from the information at hand.

For the infinite field case, radiation impedance can be considered purely resistive, but for the finite field case (i.e. transducer plus reflector which gives rise to a standing wave resonant system) the radiation impedance is complex and so in general, $Z_R = R_R + jX_R$. With reference to Figure II, 1, the input admittance can be written:

$$Y_I = \frac{1}{R_o} + j\omega C_o + \frac{1}{R + j(X_R + X)}$$

where $R = R_R + R_M$

and $X = \omega L - \frac{1}{\omega C}$

$$Y_I = G_P + j\omega C_P = \frac{1}{R_o} + \frac{R}{R^2 + (X_R + X)^2} + j\left(\omega C_o - \frac{X_R + X}{R^2 + (X_R + X)^2}\right)$$

$$\therefore G_P = \frac{1}{R_o} + \frac{R}{R^2 + (X_R + X)^2} \qquad (\text{II}, 1)$$

$$\omega C_P = \omega C_o - \frac{X_R + X}{R^2 + (X_R + X)^2} \qquad (\text{II}, 2)$$

If another medium is substituted in the standing wave system (i.e. different attenuation) then

$$G_P' = \frac{1}{R_o} + \frac{R'}{R'^2 + (X_R' + X)^2} \qquad (\text{II}, 3)$$

$$\omega C_P' = \omega C_o - \frac{X_R' + X}{R'^2 + (X_R' + X)^2} \qquad (\text{II}, 4)$$

Notice here that at a fixed frequency R_o, C_o and X stay constant since they are dependent on the properties of the transducer only.

$$\Delta G_p = G_p' - G_p = \frac{R'}{R'^2+(X_R'+X)^2} - \frac{R}{R^2+(X_R+X)^2} \qquad (II,5)$$

$$\omega\Delta C_p = \omega C_p' - \omega C_p = \frac{-(X_R'+X)}{R'^2+(X_R'+X)^2} + \frac{X_R+X}{R^2+(X_R+X)^2} \qquad (II,6)$$

$$\text{From } (II,5),\ R' = \left[\Delta G_p + \frac{R}{R^2+(X_R+X)^2}\right]\left[R'^2+(X_R'+X)^2\right] \qquad (II,7)$$

$$\text{From } (II,6),\ X_R'+X = \left[\frac{X_R+X}{R^2+(X_R+X)^2} - \omega\Delta C_p\right]\left[R'^2+(X_R'+X)^2\right] \qquad (II,8)$$

Combining (II,7) and (II,8) it can be shown that

$$R' = \frac{\Delta G_p + \dfrac{R}{R^2+(X_R+X)^2}}{\left[\Delta G_p + \dfrac{R}{R^2+(X_R+X)^2}\right]^2 + \left[\dfrac{X_R+X}{R^2+(X_R+X)^2} - \omega\Delta C_p\right]^2} \qquad (II,9)$$

$$X_R' = \frac{\dfrac{X_R+X}{R^2+(X_R+X)^2} - \omega\Delta C_p}{\left[\Delta G_p + \dfrac{R}{R^2+(X_R+X)^2}\right]^2 + \left[\dfrac{X_R+X}{R^2+(X_R+X)^2} - \omega\Delta C_p\right]^2} - X \qquad (II,10)$$

Now $R_R' = R' - R_M$ since R_M is dependent only on the properties of the transducer.

And, $R_r' = \phi^2 R_R'$ (II,11)

$X_r' = \phi^2 X_R'$ (II,12)

D. Measurement Procedures and Results.

1. Apparatus.

As mentioned previously, the experimental work was carried out with an Edo 327 transducer and styrofoam reflector (Figure II, 3). Mounted around the transducer was a frame holding three threaded rods, 120° apart, normal to the face of the transducer, and on a circle coaxial with the transducer, but outside its field pattern. The styrofoam was mounted on a backing plate through which passed the threaded rods, and which was adjusted to be parallel to the transducer face by positioning nuts on the rods. This in itself provided a certain amount of difficulty because of the convex exterior face of the transducer. It was finally decided to line up the reflector parallel to the outer edge of the transducer face on the assumption that the convex face was completely symmetrical.

In order to gain as much sensitivity as possible in the system, it was decided to place the reflector in the near field of the transducer in order to reduce to a minimum the losses caused by spherical spreading. It can be shown[3] that the last intensity maximum in the near field of a transducer occurs at an axial distance $r = a^2/\lambda$ where a = radius of transducer face (meters), and λ = wavelength of sound in the medium (meters). From this, considering the frequency range that was to be covered (40 to 100 kcs), it is determined that a separation of 10 cm between reflector and transducer would put the reflector well within the near field.

[3]Kinsler, L. E. and Frey, A. R. Fundamentals of Acoustics, 2nd Ed. Wiley and Sons, Inc., 1962: 176

TRANSDUCER-REFLECTOR SYSTEM

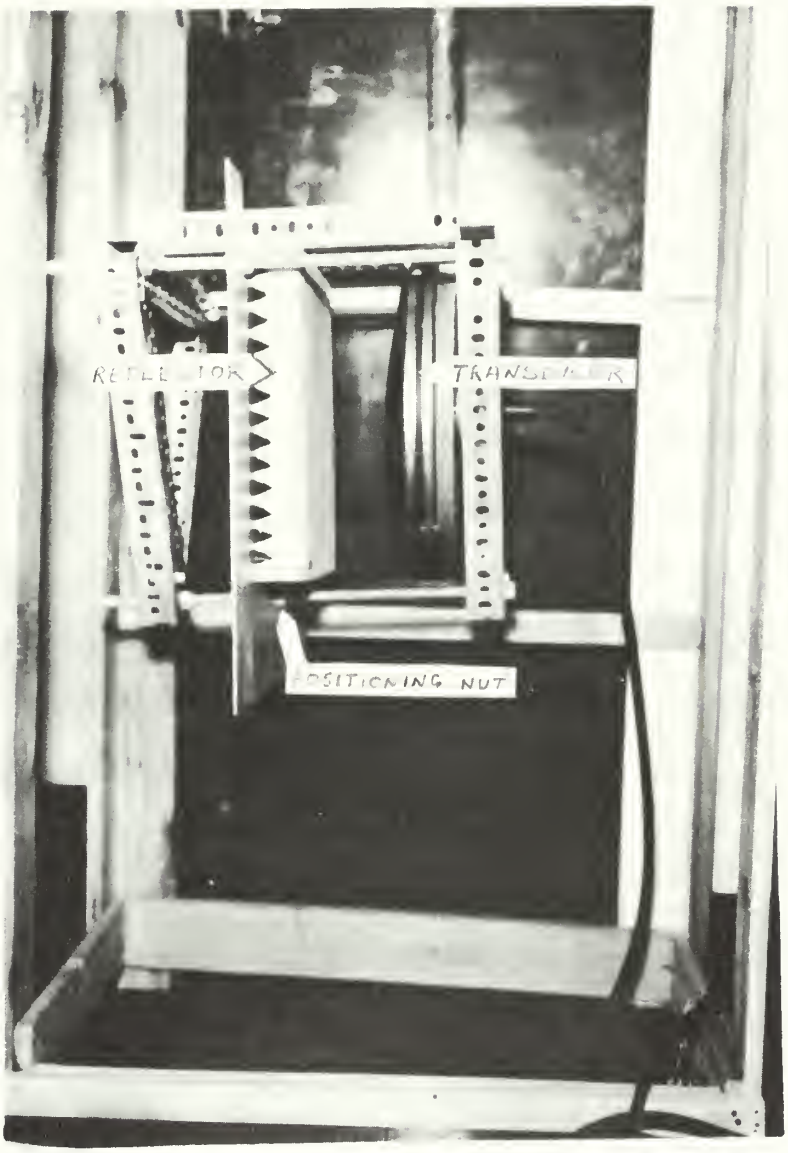

FIGURE II,3

As an aside here, it should be noted that putting the reflector in the near field causes considerable difficulty in expressing the variation of acoustic impedance with frequency; the system is no longer a simple function of the number of half wavelengths between source and reflector. These difficulties were bypassed by using a slightly different approach to the experimental method of measurement. This will be discussed in more detail later.

A bridge technique was employed for measuring the input conductance and susceptance of the experimental system as a function of frequency in bubble free and in bubbly water. A Western Electric Model 5A bridge was used in conjunction with a WE Model 17B oscillator and WE Model 2A amplifier-detector set up as shown in Figure II, 4. Rather than use the WE 2A as a detector, it was found that a better bridge balance could be obtained using a VTVM in conjunction with an oscilloscope. With this apparatus balance could be achieved to within $\pm 0{\cdot}5$ ohms and ± 10 picofards.

2. Calibration in Bubble-Free Water.

a. Bubble-free Water Production.

Bubble-free water for the calibration run was produced in a tank approximately 40 inches high by 30 inches long by 30 inches wide by heating the water as a vacuum was applied to the surface. The water was heated by means of electrical immersion heaters supplied through a sealed pipe into the tank. A flat plate was placed on top of the tank, and then clamped so as to provide an airtight seal of the air space over the water. Another pipe lead into the air space and was used to reduce the absolute pressure to about 25 inches of mercury.

BLOCK DIAGRAM OF MEASURING APPARATUS

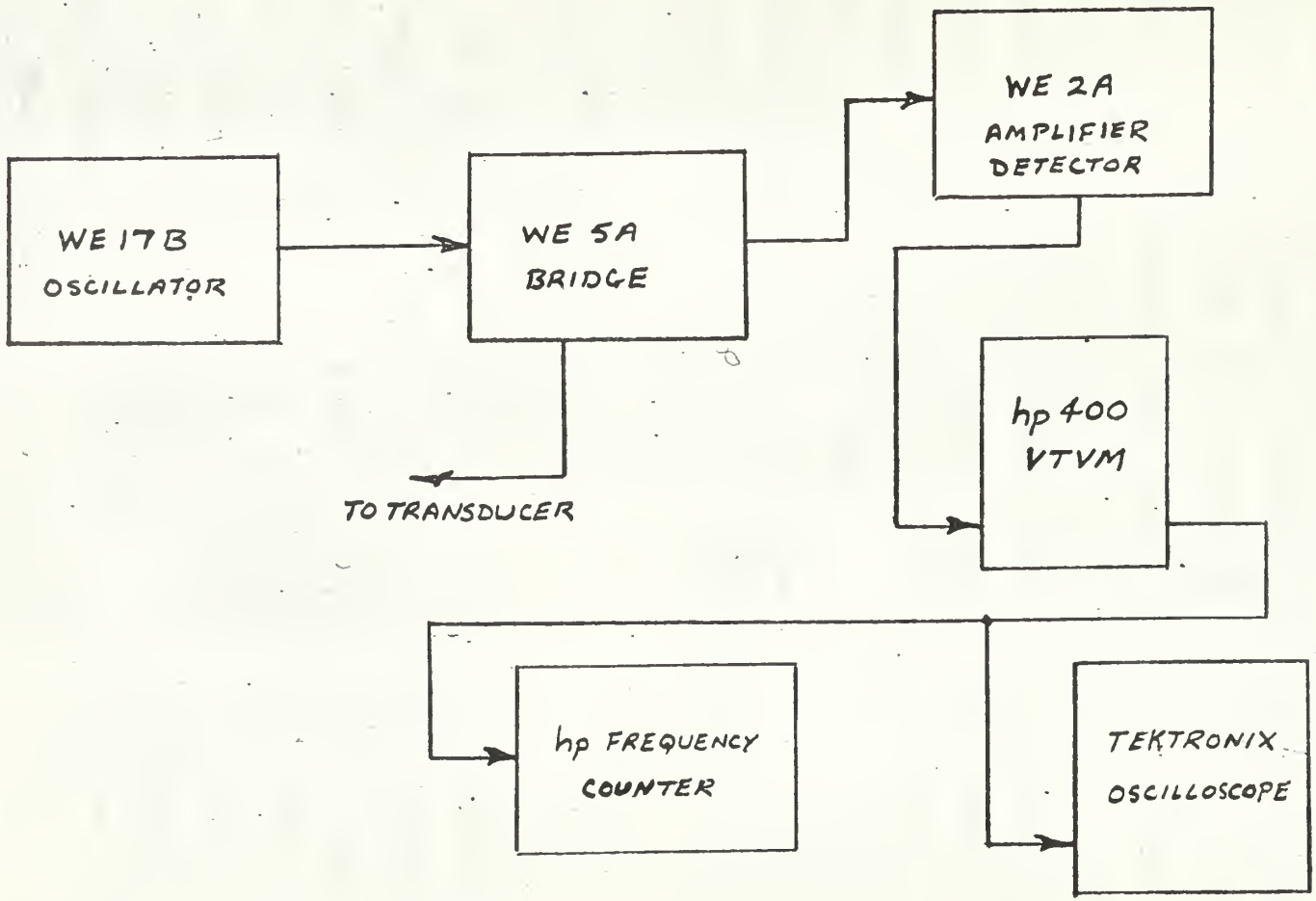

FIGURE II, 4

This was continued until all air bubbling had ceased and then the water was allowed to cool down to room temperature.

b. Calibration Procedure.

This procedure depended upon making use of the equations derived in Section C. Since the transducer characteristics had been obtained for radiation into an infinite field, values of R, X, C_p and G_p over a range of frequencies were available for use. (X_R was zero in this case because the value of ka was very much greater than one). The transducer and reflector were then placed in the bubble-free water and measurements were made of G_p' and C_p' over the same range of frequencies. A computer program, program Solve 2, contained in Appendix II, 3 was then used to solve for values of R' and X_R'. This produced for the calibration case values of R', X_R', G_p' and C_p' over a range of frequencies, and these then were designated R, X_R, G_p and C_p for use in future measurements.

3. Bubble Attenuation Measurements.

a. Measurement Procedure.

The apparatus was once more placed in the bubble-free water and micro-bubbles were introduced in the space between transducer and reflector. These bubbles were produced at the tip of a platinum wire, protuding through encasing glass, by an electrolysis process. A pulse generator, whose pulse repetition rate, pulse amplitude and pulse duration could be controlled, was used to produce bubbles of the size and number required. Once again G_p' and C_p' were determined over a range of frequencies.

b. Initial Investigations.

In the early experimental stages, G_ρ' and C_ρ' were measured at every kilocycle over the range 40 to 100 kcs. The acoustic waves from the transducer were treated as plane waves and as such the relationship between mechanical radiation impedance and attenuation could be considered as exactly that existing in acoustic interferometers [2,4,9] . In mathematical form $Z_r = S_y \rho_o c_o \frac{1 + k_r e^{-2\gamma\ell}}{1 - k_r e^{-2\gamma\ell}}$ (II ,14)

Where a = radius of transducer (meters)

k_r = reflection coefficient of the reflector

$\gamma = \alpha + j\beta$, α = attenuation (nepers per meter)

β = phase constant (radians per meter)

ℓ = distance from transducer to reflector (meters)

Then making use of this and the equations from Section C, an attempt was made to determine the attenuation caused by bubbles.

However, it soon became readily apparent that an incorrect assumption had been made when it was noticed that at certain frequencies negative attenuations were being obtained for the bubbly water, compared to the bubble-free water. Upon reconsideration it was obvious that the plane waves did not really exist in the inteferometer, a direct result of it being operated in the near field of the transducer. From the work of two authors[4,5] it can be shown that the r.m.s. pressure, averaged across an area equal to that of the transducer face, changes

[4]Seki, H., et al. Journal of the Acoustical Society of America, V.28, No. 2, Mar., 1956: 230-238

[5]Williams, A. O. Journal of the Acoustical Society of America, V.23, Jan., 1951: 1-6

in a complex manner as one moves away from the transducer in the near field. In essence this meant that equation (II, 14), was of no value for calculations with this apparatus. Some effort was made to derive the expression for variation of radiation impedance with frequency in the near field of an attenuating medium, but the project was abandoned because of the severely complex mathematics.

This early work gave rise to curves for radiation resistance such as the one shown in Figure II, 5. This particular curve was obtained for bubble-free water on one of the calibration runs. The resistance is given in units of the characteristic impedance of the water, so that the type of variation in resistance with frequency can be seen in comparison to that of the free-field case. Also shown on the curve are points representing the resistance measured for a run with bubbles in the interferometer space. The small resistance difference between bubble-free and bubbly water at each frequency gave rise to the large positive and negative attenuation swings mentioned earlier.

c. Resonant Frequency Approach.

Further study of the radiation resistance did indicate that in one way the experimental set up was acting as an interferometer in that resonant peaks appeared at 6.9 ± 0.6 kc intervals (which was the frequency interval corresponding to the interferometer separation). Since this was so, the quality factor, Q, could be found, and the attenuation calculated, near the interferometer resonant frequencies.

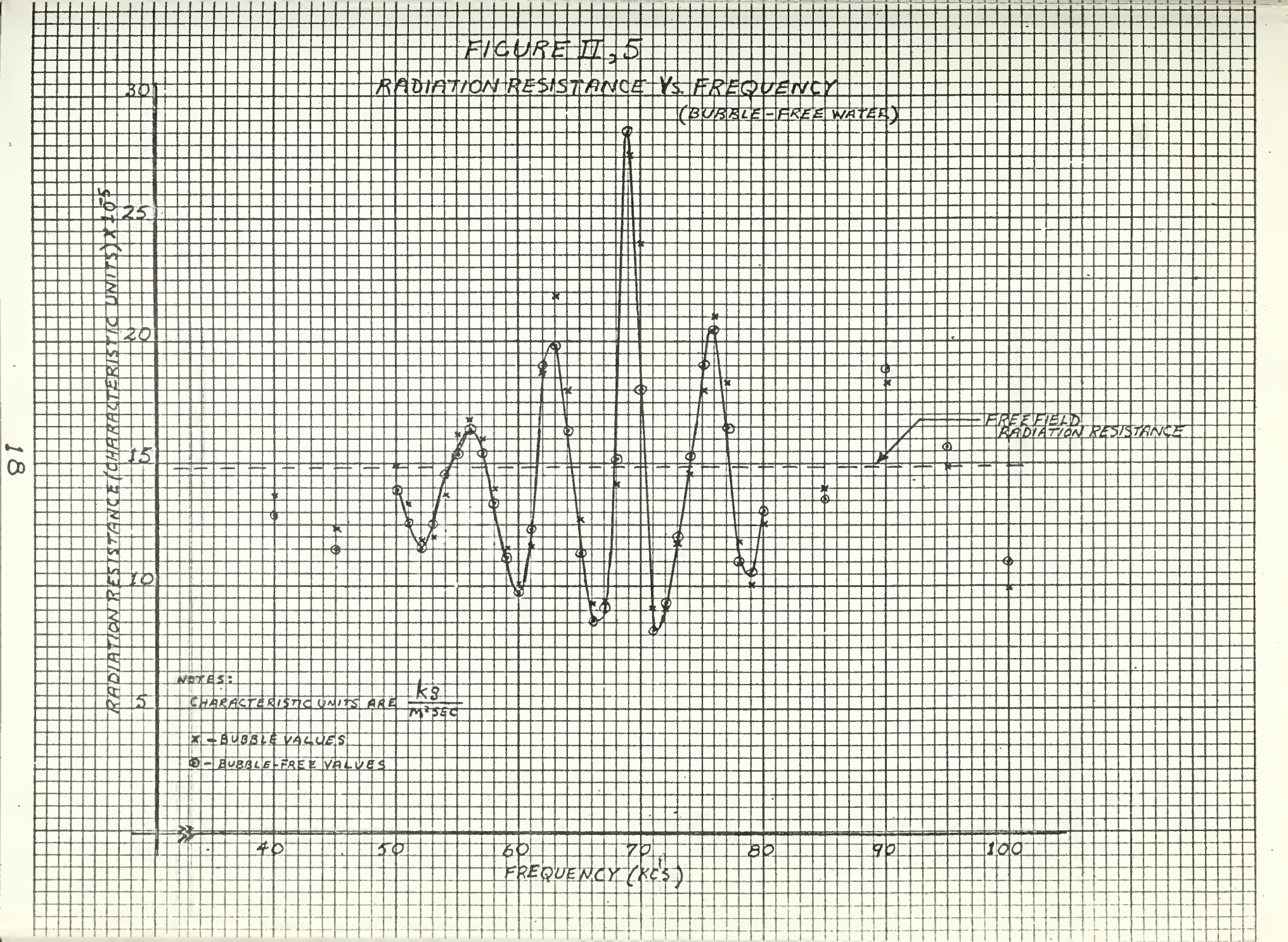
FIGURE II, 5
RADIATION RESISTANCE Vs. FREQUENCY
(BUBBLE-FREE WATER)
RADIATION RESISTANCE (CHARACTERISTIC UNITS) X 10^5
30
25
20
15
10
5
FREE FIELD RADIATION RESISTANCE
NOTES:
CHARACTERISTIC UNITS ARE kg / M²SEC
× - BUBBLE VALUES
⊙ - BUBBLE-FREE VALUES
40
50
60
70
80
90
100
FREQUENCY (KC'S)

For the bubble-free case, $Q_1 = \frac{f_o}{BW_1}$ (II,15)

where f_o = resonant frequency (kcs)

BW_1 = half power bandwidth (kcs)

and for the case of water with bubbles, $Q_2 = \frac{f_o}{BW_2}$ (II,16)

where BW_2 = half power bandwidth (kcs)

now $Q_1 = \frac{\pi}{\alpha_1 \lambda}$ (II,17)

and $Q_2 = \frac{\pi}{\alpha_2 \lambda}$ (II,18)

where α_1 = equivalent attenuation (nepers per meter) in bubble-free water

α_2 = equivalent attenuation (nepers per meter) in water with bubbles

Also if attenuation caused by bubbles alone,

$\alpha = \alpha_2 - \alpha_1$ (II,19)

Then $\alpha = \frac{\pi}{Q_2 \lambda} - \frac{\pi}{Q_1 \lambda}$ (II,20)

or $\alpha = \frac{\pi}{f_o \lambda} [BW_2 - BW_1]$ nepers per meter (II,21)

The experimental procedure for measurement was as follows. A resonant peak was selected (69.5 kcs), and measurements were made of G_p' and C_p' at 0.2 kc intervals on either side of resonance with bubbles resonant at approximately 70 kc in the space between transducer and reflector. Using the values of R, X_R, G_p and C_p found in the calibration of Section C, a computer program, Program Curve, contained in Appendix II, 3, was then used to give a readout of mechanical radiation resistance versus frequency for both the bubble-free and bubble cases. From the resonant curves then plotted, bubble attenuation at the resonant frequency could be found.

At the same time, the accuracy of the resonant frequency measurement technique was checked. A set of values for G_ρ' and C_ρ' had been obtained for a bubble run. As was mentioned earlier the accuracy in reading the WE 5A bridge was ± 0.5 ohms and ± 10 picofarads. G_ρ' and C_ρ' were then adjusted by the amount of this reading error so as to give four complete sets of data as follows:

1. G_ρ' + error and C_ρ' + error
2. G_ρ' + error and C_ρ' - error
3. G_ρ' - error and C_ρ' + error
4. G_ρ' - error and C_ρ' - error

These values were then put into a computer program, Program Curve 2, identical to Program Curve, and four readouts of radiation resistance versus frequency, corresponding to the four sets of input data, were obtained. These were then plotted, along with the original resonant curve, to determine the order of size of the variation in Q that could be expected within the limits of bridge reading accuracy. Program Curve 2 is contained in Appendix II, 3.

Typical curves of radiation resistance (mechanical ohms) around the 69.5 kc resonant point are shown for both bubble-free water, and water with bubbles in Figure II, 6. Approximately 80 to 90 bubbles, resonant at about 70 kcs, were used in the bubble run. Results were as follows: $BW_1 = 1.33$ kcs

$BW_2 = 1.72$ kcs

$Q_1 = 52.2$

$Q_2 = 40.3$

$\alpha = 0.82$ nepers per meter

For comparison it was decided to calculate the theoretical

FIGURE II, 6
69.5 KC RESONANT CURVES

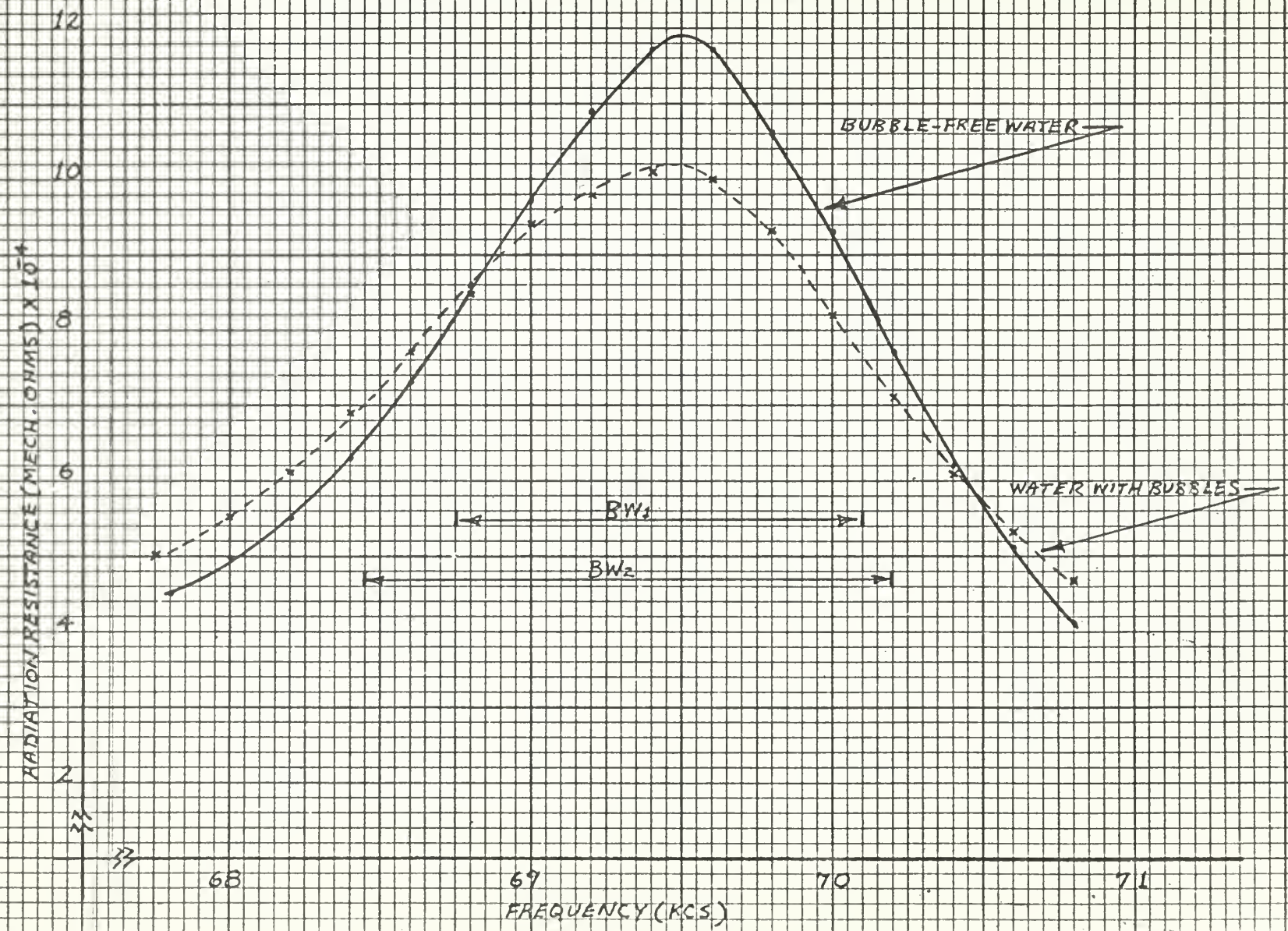

sound attenuation caused by the bubbles based upon the work described in Physics of Sound in the Sea, Part IV. [8]

At bubble resonance.

1. The extinction cross section is given by

$$\sigma_e = \frac{4\pi R^2}{\delta(kR)} \quad \text{square cms}$$

where R = bubble radius (cm)

δ = damping constant

kR = ratio of bubble circumferance to wavelength (at resonance)

2. The bubble radius is

$$R = \frac{1}{2\pi f_o}\sqrt{\frac{3\gamma P}{\rho_o}} \quad cm$$

where f_o = bubble resonance frequency (cps)

γ = ratio of specific heats

P = hydrostatic pressure (microbars)

ρ_o = density of water (grams per c.c.)

3. The attenuation in nepers per meter is

$$\alpha = \frac{1}{2} n_v \sigma_e$$

where n_v = number of bubbles per c.c.

From these data, $\alpha = 0.234$ nepers per meter. This value indicated that the experimental results were of the right order of magnitude, although much closer agreement was expected.

The smearing of the resonance curve for bubbly water, caused by the accuracy limit of the bridge readings is shown in Figure II, 7.

FIGURE II.7

69.5 KC RESONANT CURVE: VARIATION OF BANDWIDTH

(EFFECT OF BRIDGE ACCURACY)

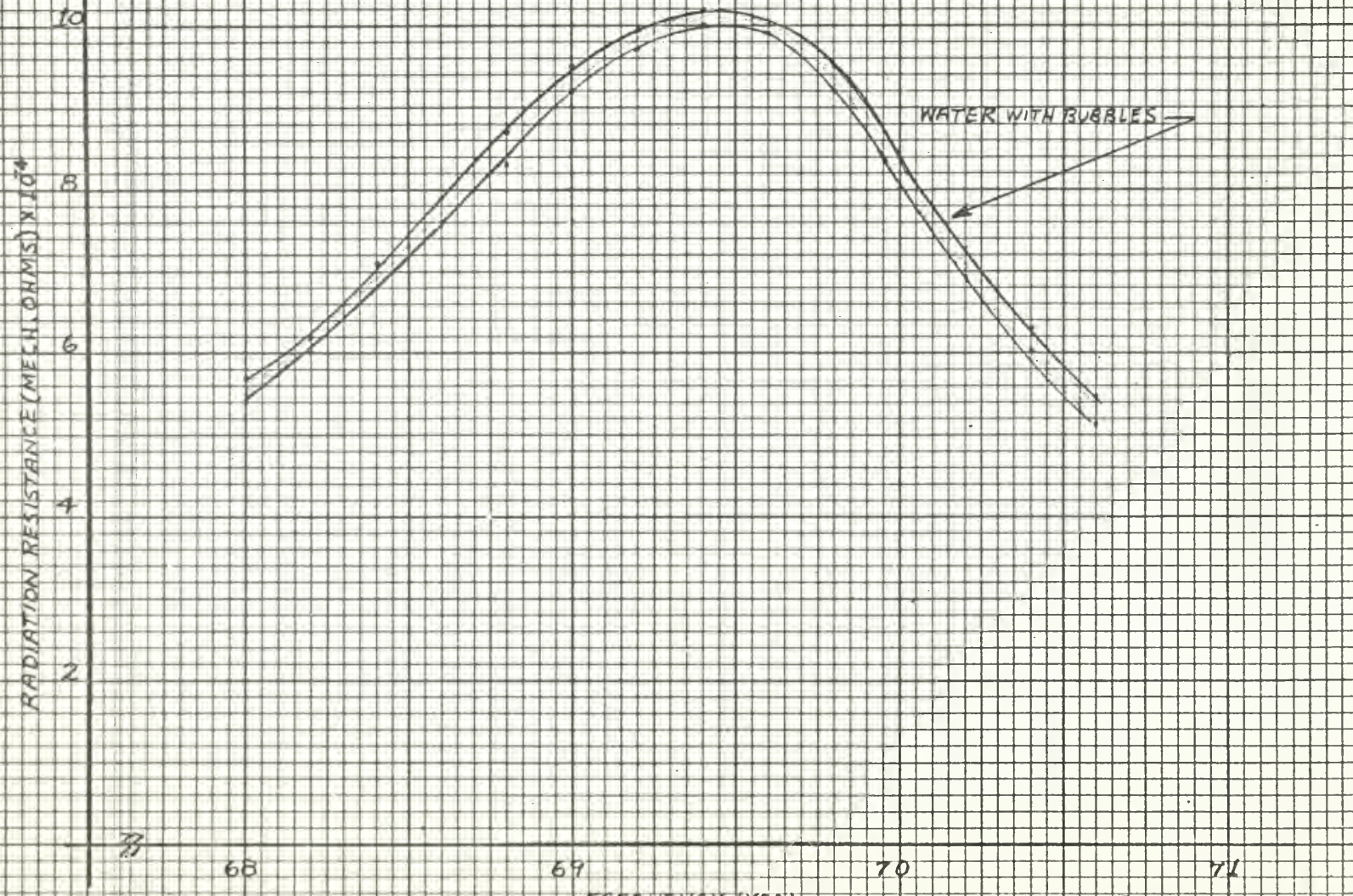

From this came the following information:

Narrowest band width = 1.7 kcs

Widest band width = 1.82 kcs

Resultant value of Q = 39.5 $\pm$ 1.3

Resultant value of α = 0.905 $\pm$ 0.125 nepers per meter

4. Auxiliary Measurements.

a. Measurement of Q by Reverberation Techniques

Initially an attempt was made to measure Q by placing a $\frac{1}{4}$ inch cylindrical probe hydrophone in the space between transducer and reflector, shutting off the oscillator periodically and observing the oscillation decay rate on an oscilloscope. It was found that this method did not work in that damping of the oscillations appeared to be instantaneous. As a check, the hydrophone was placed at various positions in the "cavity", with the same result. It was felt that the difficulty lay in the low sensitivity of the hydrophone and so another measurement method was sought.

A much more successful attempt at measurement was made using the electronic pulsing system that will be described in detail in Part III of this thesis. In this system the transmitting transducer was pulsed and then switched to receive, giving the advantage of this more sensitive receiver. The period of oscillation was maintained for long enough to excite the "cavity", then during receive time, the decay was observed on an oscilloscope.

If the decay rate is given by $e^{-\chi t}$, where χ is the temporal damping constant, then Q can be found. If the time for $e^{-\chi t}$ to decay to one half value is found then,

$$e^{-\chi t'} = \frac{1}{2}$$

$$\text{or } \chi t' = 0.693$$

$$\text{thus } \chi = \frac{0.693}{t'}$$

$$\text{Now } Q = \frac{2\pi f_o}{2\chi}$$

$$\text{or } Q = \frac{\pi f_o t'}{0.693} \qquad (II,23)$$

The time for the pulse to decay to one half its peak value was found to be $t' = 0.125$ milliseconds. From this, $Q = 39.5$, which is of the right order of magnitude. The difficulty here was that the crystal transducer would not shut off and start abruptly, resulting in some distortion of the decay envelope which made it difficult accurately to determine t'. However the order of magnitude agreement was considered to be satisfactory.

b. Apparatus Sensitivity.

A prime measure of the effectiveness of this apparatus was how few bubbles it could detect. As a check, bubbles resonant at 65 kcs were introduced into the cavity and the minimum number detectable was determined at 62 kcs (apparatus resonance), 69.5 kcs (apparatus resonance), and 65 kc. As a rule of thumb, a bridge imbalance of 2 ohms and 20 picofarads was considered to be adequate detection as this would have a noticable effect on the Q of the resonant system.

The bridge went noticeably out of balance as follows:

At 62 kc (apparatus resonance), 15 bubbles

At 65 kc, 8 to 10 bubbles

At 69.5 kc (apparatus resonance), 20 bubbles

At this point it whould be mentioned that great difficulty was experienced in controlling the resonant frequency of the bubbles generated for use in these measurements. This contributed to the uncertainity in all bubble measurements discussed here.

c. Check of "Free-field" Transducer Characteristics.

The free-field characteristics of the transducer were obtained by radiation into a supposedly anechoic sonar tank. Since these characteristics were used in all future calculations it was imperative that they be as correct as possible. A number of readings were made at selected frequencies for the transducer facing in different directions in the tank. At each frequency, all readings were checked for correlation.

It was found that the standing waves due to reflection from the tank walls caused variations in R and C as large as five ohms and 30 picofarads, respectively, depending upon orientation of the transducer axis.

This result may well be the cause of the negative attenuations mentioned earlier, and is a serious flaw in the experimental work described. It is suggested that this effect should be investigated further, reduced to a minimum, and then a check made to see if the negative attenuations still exist.

d. Temperature Effects.

All the measurements carried out in the laboratory were performed in water at 22-23°C. Since the ocean could be expected to differ from this temperature, a bubble-free calibration was made at 18°C and checked against the run at 23°C to see if any radical changes occurred in the measured parameters.

It was found that significant changes do occur, and hence the system must be calibrated at the temperature at which it will be used.

E. Comment and Discussion.

1. Attenuation Measurement Accuracy.

The experimental results indicated that attenuation caused by bubbles could be determined using the resonant frequency curve approach. Q's were high enough to give a narrow bandwidth and reasonable selectivity, resulting in the apparatus being named a bubble spectrometer.

In order to discuss the accuracy of attenuation measurement it is necessary to consider the relative attenuation caused by a bubble at frequencies near its resonance peak. The bubble scattering cross section at any frequency relative to bubble resonance scattering cross section is given by[6] $\frac{\sigma_s(\omega)}{\sigma_s(\omega_o)} = \frac{\delta^2(\omega_o)}{\left[\left(\frac{f_o}{f}\right)^2 - 1\right] + \delta^2(\omega)}$ where δ is a damping constant which varies with frequency.[7]

Near resonance $\frac{\sigma_s(\omega)}{\sigma_s(\omega_o)} \simeq \frac{1}{\left(2\frac{\Delta f}{f_o \delta}\right)^2 + 1}$, where $\Delta f = f - f_o$.

Choosing $\delta \simeq 0.1$, a plot of relative scattering cross section versus $\frac{\Delta f}{f_o}$ has a relative width of approximately 0.09.

The accuracy of the attenuation measurement depends upon attenuation, α , being constant across the bandwidth of the bubble spectrometer. Since $\frac{\alpha(\omega)}{\alpha(\omega_o)}$ varies directly as $\frac{\sigma_s(\omega)}{\sigma_s(\omega_o)}$, relative attenuation can be plotted as a function of $\frac{\Delta f}{f_o}$. Figure II, 8 shows attenuation in arbitrary units plotted against frequency at $f_o = 67kc$ and $f_o = 70kc$, and superimposed over the bubble

[6]Physics of Sound in the Sea, Division 6, Volume 8, NDRC Summary Technical Reports: 466

[7]Devin, C., Journal of the Acoustical Society of America, V. 31, 1959: 1654

FIGURE II, 8

ATTENUATION VARIATION ACROSS SPECTROMETER BANDWIDTH

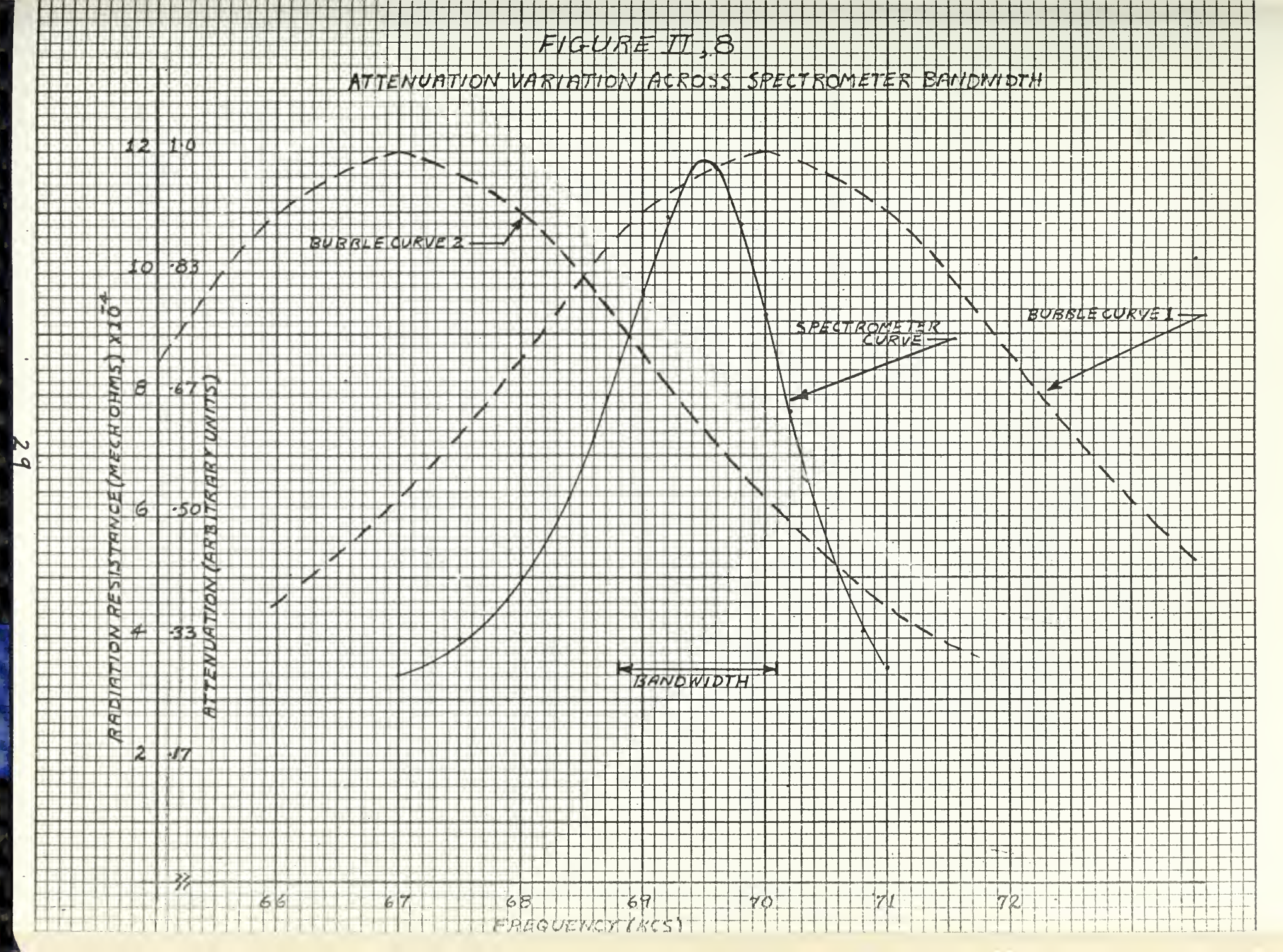

spectrometer curve resonant at 69.5 kc. From this it can be seen that,depending upon the distance (in frequency) of bubble resonance from spectrometer resonance, attenuation will vary a small or large amount across the spectrometer band width.

As a comment here it should be noted that in the experimental work, the experimenter was fortunate to have bubbles resonant at approximately 70 kc, giving rise to a large attenuation, almost constant across the spectrometer band width centered at 69.5 kc.

As can be seen this rapidly varying attenuation property of a single bubble could lead to many difficulties in the laboratory if accurate calibration of the spectrometer was desired. At sea, however, the problem would be non-existent since a distribution in bubble size would exist giving rise to large scale flattening of the attenuation versus frequency curves, and an apparently flat attenuation value across the spectrometer band width.

2. Measurement Sensitivity.

From the results obtained using bubbles of 65 kc resonant size, it would appear that in the worst case a volume concentration of bubbles of 6.4×10^{3} bubbles per cubic meter, or 20 bubbles in the "cavity" would be required for any attenuation measurement. Expressed another way, this bubble concentration is equal to of the order of 3×10^{-9} bubble volume per volume of liquid. Studies of air bubbles in wakes of destroyers[8] have resulted in the detection of bubble volumes per liquid volume of the order of 10^{-7}, the bubbles being distributed in size.

[8]Physics of Sound in the Sea, Division 6, Volume 8, NDRC Summary Technical Reports: 534

3. Serious Experimental Disadvantages.

a. As indicated earlier, true free field characteristics were not obtained in the supposedly "anechoic" sonar tank. Since all following calculations were based upon the free-field measurements it can be seen that this fault will have to be corrected before proper and complete evaluation can be made of the experimental method. It remains to be seen whether or not the negative attenuations obtained in the early experimental work were a result of this defect, rather than a results of assuming plane waves in the near field of the transducer. In order to obtain true free-field characteristics of the transducer, measurements would have to be made in a bubble-free ocean or in a truly anechoic environment to avoid the reflection that occurred in the sonar tank.

b. The effect of bridge reading accuracy at present places a serious limitation on the experimental technique. In the results, the variation of attenuation per unit length for one particular bubble run was shown to be 0.905 ± 0.125 nepers per meter. Now this inaccuracy in itself is very bad, but there is yet another consideration which has been ingnored up to now. For the bubble-free calibration case, the mechanical radiation resistance and reactance were assumed to be exactly correct. In reality they would have the same type of uncertainty as the bubble run readings. This then would have two effects. First, the Q for the calibration case would also be "smeared", and second, since the calibration case readings are used in calculating radiation resistance for the bubble run, a further spreading of the bubble run Q curve would occur.

c. The overall conclusion here is that in its present form the bubble spectrometer requires various improvements before it can be considered to be an effective device. In addition to improvement of the anechoic environment for free field measurements, use of a more accurate bridge might well alleviate the problem. In the laboratory, very accurate balance could be obtained, but this usually involves using a very sensitive galvanometer. This then would present an almost insurmountable problem at sea. It would seem that the best indicator that could be of service at sea would be an oscilloscope used in conjunction with a more finely balancing bridge.

4. Other Limitations.

a. With a fixed separation between transducer and reflector, attenuation can only be measured at each of the resonant peaks, that is, at approximately seven kc intervals. This would be no disadvantage at sea where the bubble size is distributed over a wide range of values. However, it is a disadvantage in the laboratory, if the system is to be accurately calibrated.

b. At each resonant peak area it takes about 10 to 12 readings at small frequency intervals to obtain a usable resonant curve. This does present a serious disadvantage in that the transducer is sensitive to motion, making balance of the bridge under these conditions a delicate matter. This may well be the case at sea when trying to make readings while the vessel in use rolls and/or pitches. Here instantaneous readings are almost a must.

c. The transducer in use had a very non-uniform response

pattern making its use outside the range 40-150 kcs completely inpracticable. The frequency range over which accurate results could be obtained was far less than that. The characteristics of the transducer were obtained from motional admittance circles drawn for data 20-30 kc on each side of the transducer resonance (67.8 kc). Far from resonance, these characteristics change[9], and thus would introduce errors into calculations made at these remote frequencies (below 40 kc and above 100 kc).

d. The experimental results indicated the temperature sensitivity of the transducer. In order to avoid the influence of temperature effects, the transducer free field measurements and the calibration run would have to be carried out at the same temperature as the bubble measuring run. The reasons for the temperature sensitivity of the device can be readily explained as follows. With a change in temperature the ρc of the water changes[10] having an effect on the radiation impedance of the transducer. Also, since the transducer used was a piezoelectric type, with changes in temperature sound velocity in the crystal changes, thus changing the stiffness[11]. In effect this changes the value of the motional capacitance of the transducer. It is the combination of these two effects that causes the temperature sensitivity.

[9]Kinsler, L. E. and Frey, A. R. Fundamentals of Acoustics, 2nd Ed. Wiley and Sons, Inc., 1962: 342

[10]Dorsey, Properties of Ordinary Water Substance, Reinhold Publishing Corp., 1940: 192, 199

[11]Hueter, T. F. and Bolt, R. H., Wiley and Sons Inc., 1955: 124

APPENDIX II, 1

EDO MODEL 327 SONAR TRANSDUCER

The Edo Model 327 transducer is an underwater, electroacoustic unit designed to be used as a general purposes projector or hydrophone, and as a reciprocal transducer in a reciprocity calibration. The unit is effectively a piston radiator which may be driven by as much as 100 watts under steady - state conditions with a water load at frequencies from 5 to 150 kc. The active element is an array of ADP crystals.

The transducer is cylindrical in shape. It consists of a nickel plated brass housing, crystal array, acoustically transparent rubber cover, cable and cable gland seal. The weight of the transducer and its cable in air is 36 pounds.

The crystal array, which is cemented to a corprene and aluminum backing plate, is mounted within the housing and faces the rubber window. This acoustically transparent window covers the entire front surface of the assembly and seals the transducer. De-aerated, moisture-free castor oil fills the compartment between the window and the crystal array. The crystals are grouped into two independent arrays, an inner one at the center of the array face and a wide outer circular row which gives a narrow beam when operated in parallel with the inner group.

APPENDIX II, 2

EDO 327 TRANSDUCER CHARACTERISTICS IN ELECTRICAL UNITS

R_o = 7700 ohms

R_R = 1265 ohms (free field in water)

R_M = 1175 ohms

C_o = 6480 picofarads

C = 622 picofarads

L = 8.89 millihenries

ϕ^2 = 42.8

S_y = 3.66×10^{-2} square meters

APPENDIX II,3

```
      PROGRAM SOLVE 2
C     PROGRAM TO OBTAIN RADIATION+MOTIONAL RESISTANCE AND RADIATION
C     REACTANCE FOR TRANSDUCER IN BUBBLE FREE WATER. THIS DATA IS USED
C     AS A CALIBRATION STANDARD
      READ2,NOPTS
    2 FORMAT(I5)
      PRINT1000
C     FREQ=FREQUENCY(CPS)
C     RADR=RADIATION RESISTANCE(BUBBLE FREE WATER)
C     RADX=RADIATION REACTANCE(BUBBLE FREE WATER)
 1000 FORMAT(1H1///7X,4HFREQ,13X,4HRADR,14X,4HRADX///)
      DO100I=1,NOPTS
C     A=RADIATION REACTANCE(FREE FIELD)
C     B=TRANSDUCER MOTIONAL REACTANCE
C     C=RADIATION RESISTANCE + MOTIONAL RESISTANCE(FREE FIELD)
C     PP=FREQUENCY(CPS)
C     RIN=BRIDGE RESISTANCE(FREE FIELD)
C     CP=BRIDGE CAPACITANCE(FREE FIELD)
C     RINI=BRIDGE RESISTANCE(BUBBLE FREE WATER)
C     CPI=BRIDGE CAPACITANCE(BUBBLE FREE WATER)
      READ2000,A,B,C,PP,RIN,CP,RINI,CPI
 2000 FORMAT(8E9.4)
C     RO=BRIDGE RESISTANCE CONSTANT FACTOR
      RO=1000.
      GPI=(RO-RINI)/(RO*RINI)
      GP=(RO-RIN)/(RO*RIN)
      G=CPI-CP
      D=GPI-GP
     OR=(C/(C**2+(A+B)**2)+D)/(((A+B)/(C**2+(A+B)**2)-6.2832*PP*G)**2+(C
     1/(C**2+(A+B)**2)+D)**2)
     OZ=((A+B)/(C**2+(A+B)**2)-6.2832*PP*G)/(((A+B)/(C**2+(A+B)**2)-6.28
     132*PP*G)**2+(C/(C**2+(A+B)**2)+D)**2)-B
      PRINT3000,PP,R,Z
 3000 FORMAT(1H0,1E12.6,7X,1E12.6,7X,1E12.6)
  100 CONTINUE
      END
      END
```

```
      PROGRAM CURVE
C     PROGRAM TO COMPARE RESONANCE CURVES FOR BUBBLE FREE WATER AND
C     FOR WATER WITH BUBBLES AND FROM THE DIFFERENCE IN Q FIND THE
C     ADDED ATTENTION CAUSED BY BUBBLES.
      READ2,NOPTS
    2 FORMAT(I5)
      PRINT 1000
10000 FORMAT(1H1///6X4HFREQ,15X,4HRRBF,15X,4HRRWB,15X,4HRXBF,15X,4HRXWB/
     1//)
C     FREQ=FREQUENCY(CPS)
C     RRBF=RADIATION RESISTANCE(BUBBLE FREE WATER)
C     RRWB=RADIATION RESISTANCE(WATER WITH BUBBLES)
C     RXBF=RADIATION REACTANCE(BUBBLE FREE WATER)
C     RXWB=RADIATION REACTANCE(WATER WITH BUBBLES)
      DO100I=1,NOPTS
      READ2000,A,B,C,PP,RIN,CP,RINI,CPI
 2000 FORMAT(8E9.4)
C     A=RADIATION REACTANCE(BUBBLE FREE WATER)
C     B=TRANSDUCER MOTIONAL REACTANCE
C     C=RADIATION RESISTANCE+MOTIONAL RESISTANCE(BUBBLE FREE WATER)
C     PP=FREQUENCY(CPS)
C     RIN=BRIDGE RESISTANCE(BUBBLE FREE WATER)
C     CP=BRIDGE CAPACITANCE(BUBBLE FREE WATER)
C     RINI=BRIDGE RESISTANCE(WATER WITH BUBBLES)
C     CPI=BRIDGE CAPACITANCE(WATER WITH BUBBLES)
      RO=1000.
C     RO=BRIDGE RESISTANCE CONSTANT FACTOR
      GPI=(RO-RINI)/(RO*RINI)
      GP=(RO-RIN)/(RO*RIN)
      G=CPI-CP
      D=GPI-GP
      ALFA=C/(C**2+(A+B)**2)+C
      BETA=(A+B)/(C**2+(A+B)**2)-6.2832*PP*G
      R=ALFA/((ALFA)**2+(BETA)**2)
      Z=BETA/((ALFA)**2+(BETA)**2)-B
      W=(C-1175.)*42.8
      U=(R-1175.)*42.8
      Y=A*42.8
      V=Z*42.8
      PRINT3000,PP,W,U,Y,V
 3000 FORMAT(1HO,1E12.6,7X,1E12.6,7X,1E12.6,7X,1E12.6,7X,1E12.6)
  100 CONTINUE
      END
      END
```

```
      PROGRAM CURVE 2
C     THIS PROGRAM CHECKS THE ACCURACY OF PROGRAM CURVE
      READ2,NOPTS
    2 FORMAT(I5)
      PRINT 1000
 10000FORMAT(1H1///6X4HFREQ,15X,4HRRBF,15X,4HRRWB,15X,4HRXBF,15X,4HRXWB/
     1//)
C     FREQ=FREQUENCY(CPS)
C     RRBF=RADIATION RESISTANCE(BUBBLE FREE WATER)
C     RRWB=RADIATION RESISTANCE(WATER WITH BUBBLES)
C     RXBF=RADIATION REACTANCE(BUBBLE FREE WATER)
C     RXWB=RADIATION REACTANCE(WATER WITH BUBBLES)
      DO100I=1,NOPTS
      READ2000,A,B,C,PP,RIN,CP,RINI,CPI
 2000 FORMAT(8E9.4)
C     A=RADIATION REACTANCE(BUBBLE FREE WATER)
C     B=TRANSDUCER MOTIONAL REACTANCE
C     C=RADIATION RESISTANCE+MOTIONAL RESISTANCE(BUBBLE FREE WATER)
C     PP=FREQUENCY(CPS)
C     RIN=BRIDGE RESISTANCE(BUBBLE FREE WATER)
C     CP=BRIDGE CAPACITANCE(BUBBLE FREE WATER)
C     RINI=BRIDGE RESISTANCE(WATER WITH BUBBLES)
C     CPI=BRIDGE CAPACITANCE(WATER WITH BUBBLES)
      RO=1000.
C     RO=BRIDGE RESISTANCE CONSTANT FACTOR
      GPI=(RO-RINI)/(RO*RINI)
      GP=(RO-RIN)/(RO*RIN)
      G=CPI-CP
      D=GPI-GP
      ALFA=C/(C**2+(A+B)**2)+D
      BETA=(A+B)/(C**2+(A+B)**2)-6.2832*PP*G
      R=ALFA/((ALFA)**2+(BETA)**2)
      Z=BETA/((ALFA)**2+(BETA)**2)-B
      W=(C-1175.)*42.8
      U=(R-1175.)*42.8
      Y=A*42.8
      V=Z*42.8
      PRINT3000,PP,W,U,Y,V
 3000 FORMAT(1H0,1E12.6,7X,1E12.6,7X,1E12.6,7X,1E12.6,7X,1E12.6)
  100 CONTINUE
      END
      END
```

III

PULSE ECHO SYSTEM FOR ATTENUATION MEASUREMENT

A. General.

The investigation of a pulse-echo system for attenuation measurement was undertaken when initial efforts in the direction of an acoustic transmission line method indicated possible complications. The general concept was to mount a transducer and a reflector in an open framework with free circulation of the sea water through the transducer-reflector space. The multiple echoes in this system would provide an effective path length many times greater than the transducer to reflector spacing. In addition, this system would offer a capability for sound velocity measurements.

It was desired that the system be capable of measuring attenuation due to microbubbles in the frequency range of 20 kcs to 150 kcs. It was further desired that a relatively large volume of water be involved in the measurement since the distribution of bubbles in sea water was unknown. A consideration of these requirements led to the selection of an electrostatic (solid dielectric) transducer of 25 to 30 cm diameter. This type of transducer is analogous to the condenser microphone and is characterized by a flat output over a wide frequency and, consequently, by good pulse response. The requirements for this phase of the project thus became to design and construct an electrostatic transducer, incorporate this transducer into a pulse-echo system, and to determine the effectiveness of this technique in measuring bubble attenuation in water.

B. The Electrostatic Transducer.

1. Brief Theory.

Descriptions of electrostatic transducers may be found in a number of publications [2, 4, 24]. Work on electrostatic transducers with solid dielectric for waterborne sound has been reported by G. R. Shodder and F. Wiekhorst [25]. A simple derivation will be used here to obtain the expected forms of the receiving and transmitting sensitivities of an electrostatic transducer. This type of transducer with diameter large in comparison to a wavelength, when used in water, may be considered as a resistance controlled mechanical system with equation of motion given by equation (III, 1), where R is mechanical resistance, χ is displacement, and F is the driving force.

$$R \frac{\partial \chi}{\partial t} = F \qquad \text{(III, 1)}$$

Considering the transducer as a receiver the force may by replaced by the pressure, p, times the area, A. The harmonic solution of equation (III, 1) in terms of magnitudes only is given by equation (III, 2) where ω is angular frequency.

$$R \omega \chi = p A \qquad \text{(III, 2)}$$

If a large polarizing voltage is applied such that the total charge remains essentially constant, then the alternating voltage developed, v, is approximately proportional to the displacement. When this is substituted in equation (III, 2) the microphone sensitivity is obtained as

$$M = \frac{v}{p} = \frac{\text{Constant}}{\omega} \qquad \text{(III, 3)}$$

Considering the transducer as a transmitter with driving current i, the ratio $S=\frac{P}{i}$ is called the transmitter sensitivity. Using equation (III, 3) and the fact that $i = \omega C v$, where C is the capacitance, the transmitter sensitivity is obtained as

$$S = \frac{P}{i} = \text{Constant} \qquad \text{(III, 4)}$$

It is seen from this derivation that as a receiver, the voltage output of the electrostatic transducer is proportional to one over the frequency for constant incident pressure, and as a transmitter the pressure is constant with frequency for constant driving current. If the diameter of the transducer is comparable to the wavelength or small compared to the wavelength, then the above equations are no longer valid and a more detailed analysis must be undertaken. In the frequency range of this project (20-150kcs) the results obtained with an experimental transducer are in agreement with the resistance-control assumption and the conclusions of equations (III, 3) and (III, 4).

2. Transducer Design and Construction.

A cross-sectional view of the actual transducer is shown in Figure III, 1. The aluminum plate is the fixed electrode, the mylar is the solid dielectric and the movable electrode is a thin aluminum coating on the outer side of the mylar. Electrical contact is made to the fixed electrode through a stuffing tube and to the movable electrode by silver paint. A small air cushion exists between the fixed electrode and the mylar. The grooves in the fixed electrode increase this air cushion and add to the compliance of the system with the effect of increasing the sensitivity. This design also

employs pressure equalization as described by H. Kuttruff and P. Wille [22]. The purpose of this equalization is to improve the uniformity of transducer sensitivity as operating depth is changed, by acting to keep the volume of air constant. A supply of aluminum-coated mylar which was readily available allowed a transducer to be constructed with a diameter of 24 cm and since this gives a diameter to wavelength ratio of eight at 50 kcs this diameter was considered satisfactory. The mylar was installed by clamping it in a frame which could then be used to stretch the mylar over the fixed electrode with an epoxy bond being made between the mylar and the Plexiglas rim.

A coating was required to protect the thin aluminum surface on the mylar from the action of sea water. This coating has negligible effect on transducer performance provided that its mass is not excessive, its thickness is much less than a quarter wavelength, and it does not contain air bubbles. Using 200 kcs as an upper frequency, calculations showed that a thickness of 0.5 mm would be acceptable with respect to the quarter wavelength criterion. The experimental results show that the added mass did not effect the resistance-control assumption for frequencies to 150 kcs. A Shell epoxy resin, Epon 828, was selected and several methods were investigated for obtaining the desired coating. A form was constructed to allow the epoxy to be poured and leveled to the desired thickness. It was thought at first that a vacuum should be used to ensure the removal of all air bubbles from the coating. A slow-setting curing agent (Shell curing agent D) was used and several different pressures were

tried. In all cases there was considerable outgassing of the epoxy and the bubbles formed at the surface caused many bare areas to develop. With a 0.5mm coating the use of vacuum did not appear practical. It was observed that if care was used in mixing and pouring the epoxy a coating could be obtained which appeared to be free of entrained air bubbles. An acceptable coating was thus obtained at room pressure using Epon 828 and curing agent U. This coating remained in satisfactory condition after a period of several months during which the transducer was used extensively.

3. Results.

The transmitting and receiving sensitivities obtained with this experimental transducer are shown in Figure III, 2. The transmitting sensitivity is essentially constant in accordance with equation (III, 4) and the receiving sensitivity decreases at nearly 6db per octave as predicted by equation (III, 3). These curves were obtained with a dc polarizing voltage of 200 volts; the fixed electrode was positive with respect to the movable electrode. If the polarizing voltage were to be increased the sensitivities would increase. When used as a transmitter the alternating voltage should be small compared to the polarizing voltage in order to reduce harmonic distortion. With 200 volts polarizing voltage it was considered that the driving voltage should be maintained at a maximum of 20 volts peak value. Sound pressure levels, referred to 1 meter, with this maximum driving voltage were 55.9 db re 1 microbar at 20 kcs and 68.7 db at 100 kcs.

The fairly large diameter of this transducer makes it highly directive as evidenced by the 50 kcs and 100 kcs horizontal radiation

patterns Figure (III, 3) and Figure (III, 4). The locations of the nulls and peaks in the radiation patterns agree closely with those predicted for a flat circular piston [6].

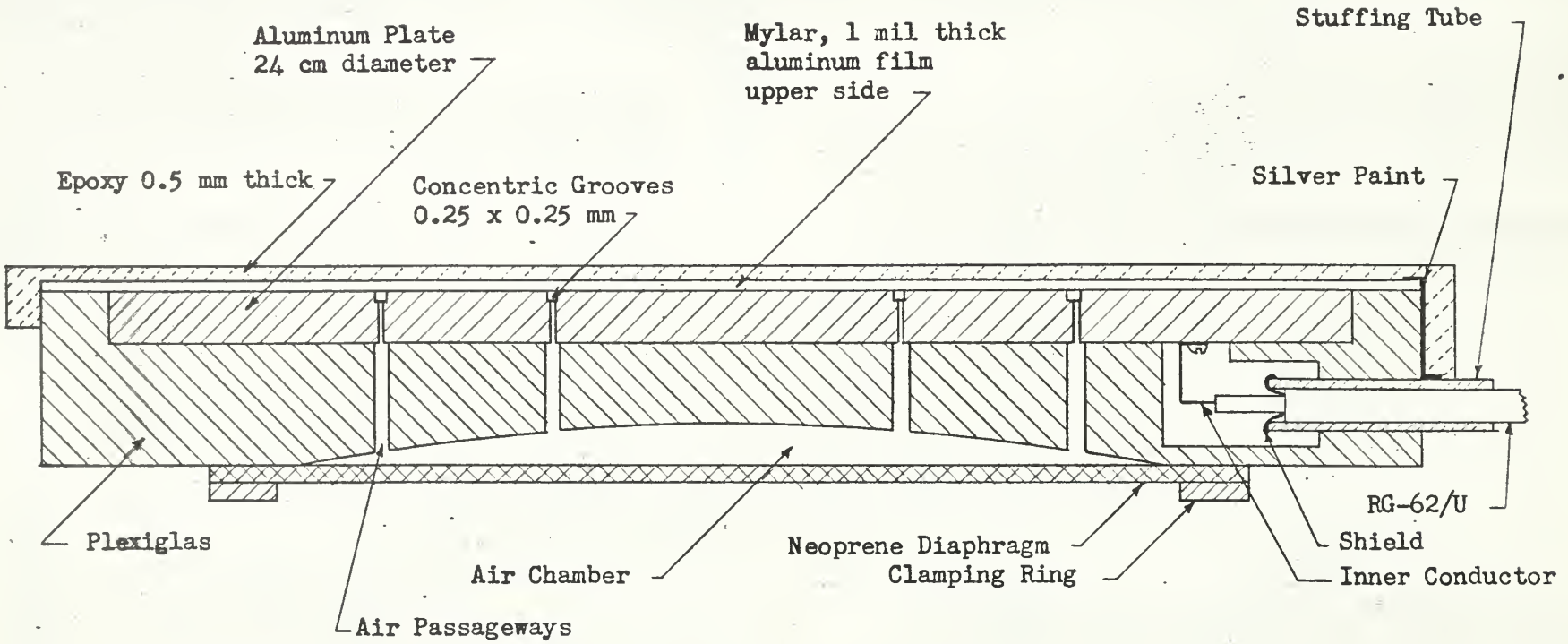

Figure III.1 Electrostatic Transducer Cross-Sectional View (Not to scale)

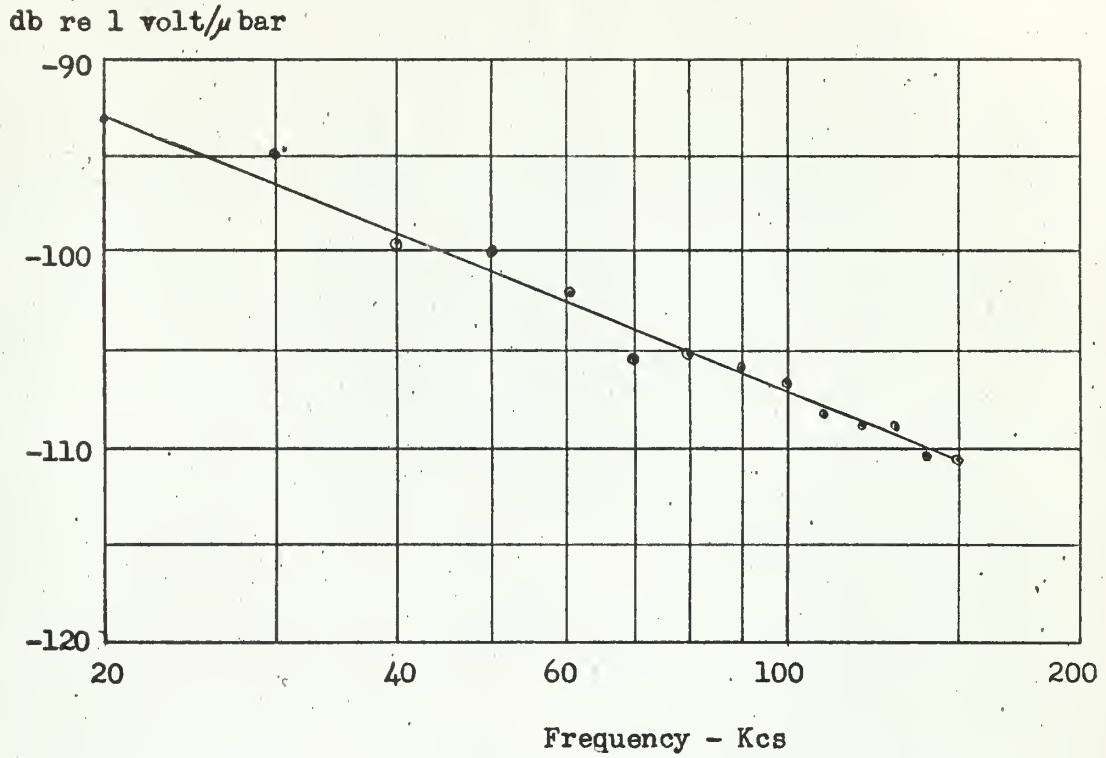

(a) Receiving Sensitivity

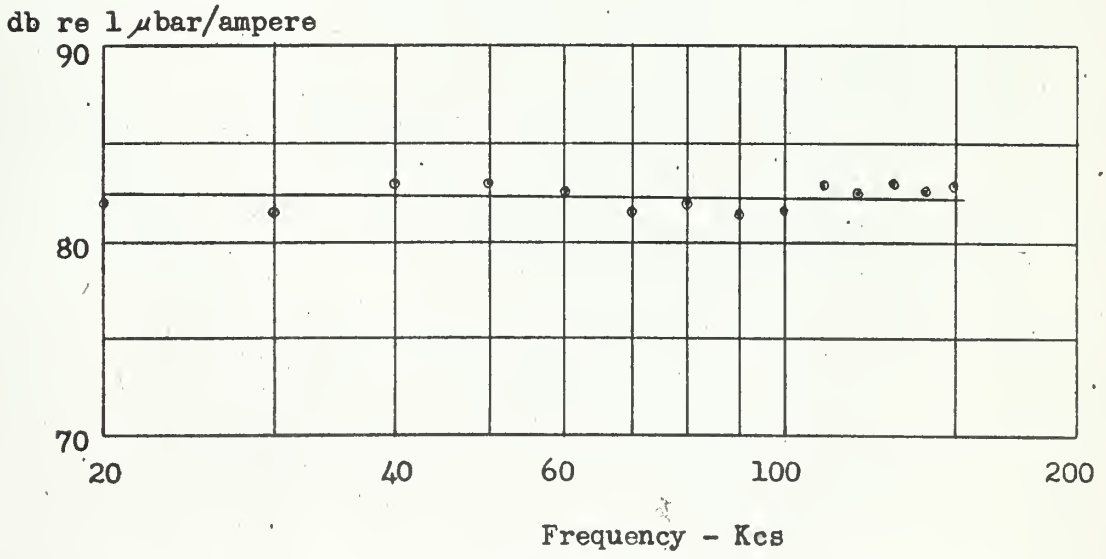

(b) Transmitting Sensitivity (at 1 meter)

Figure III.2 Electrostatic Transducer Receiving & Transmitting Sensitivities (Polarizing Voltage = 200 volts)

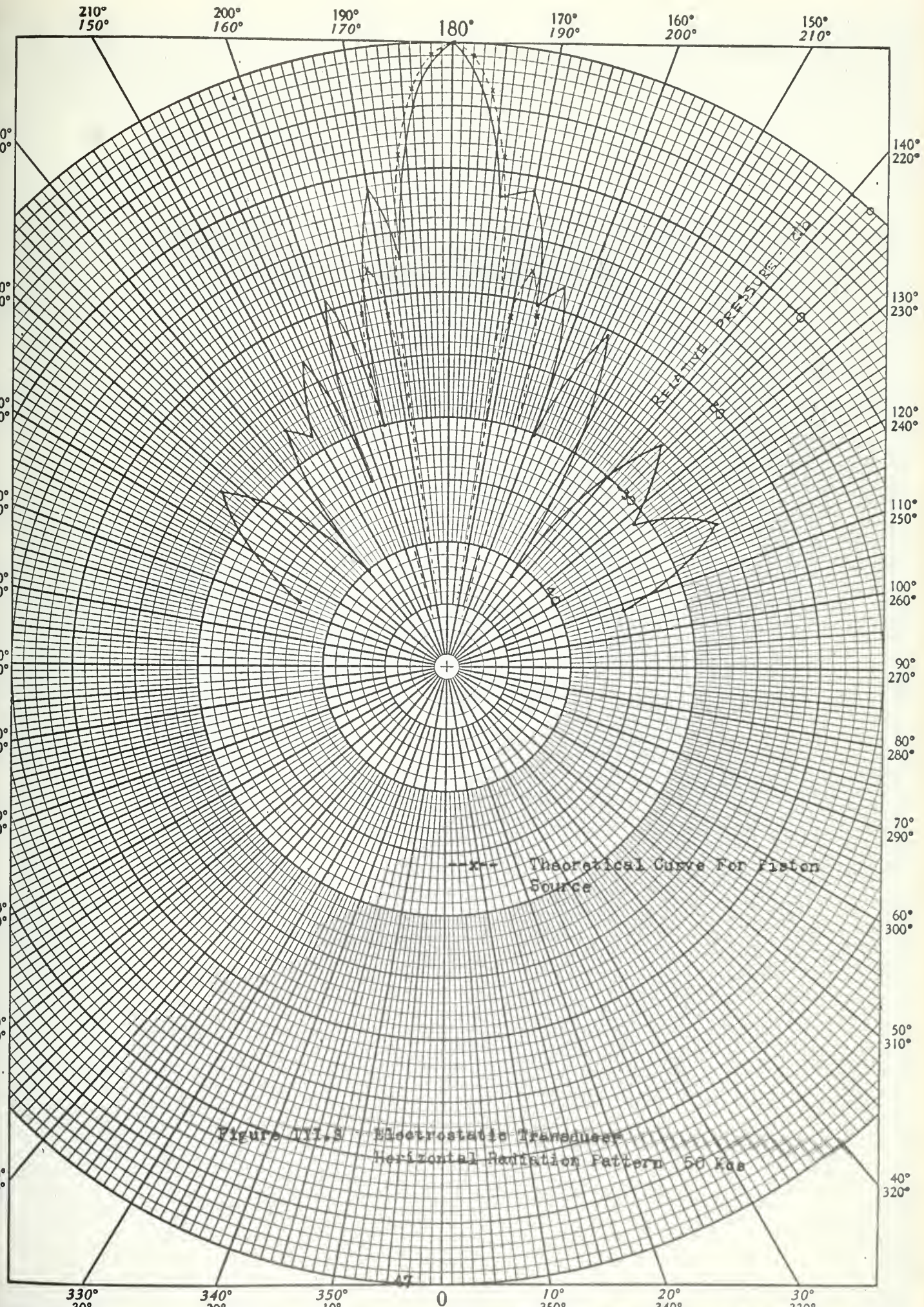

Figure VII.8 Electrostatic Transducer
Horizontal Radiation Pattern 50 Kcs

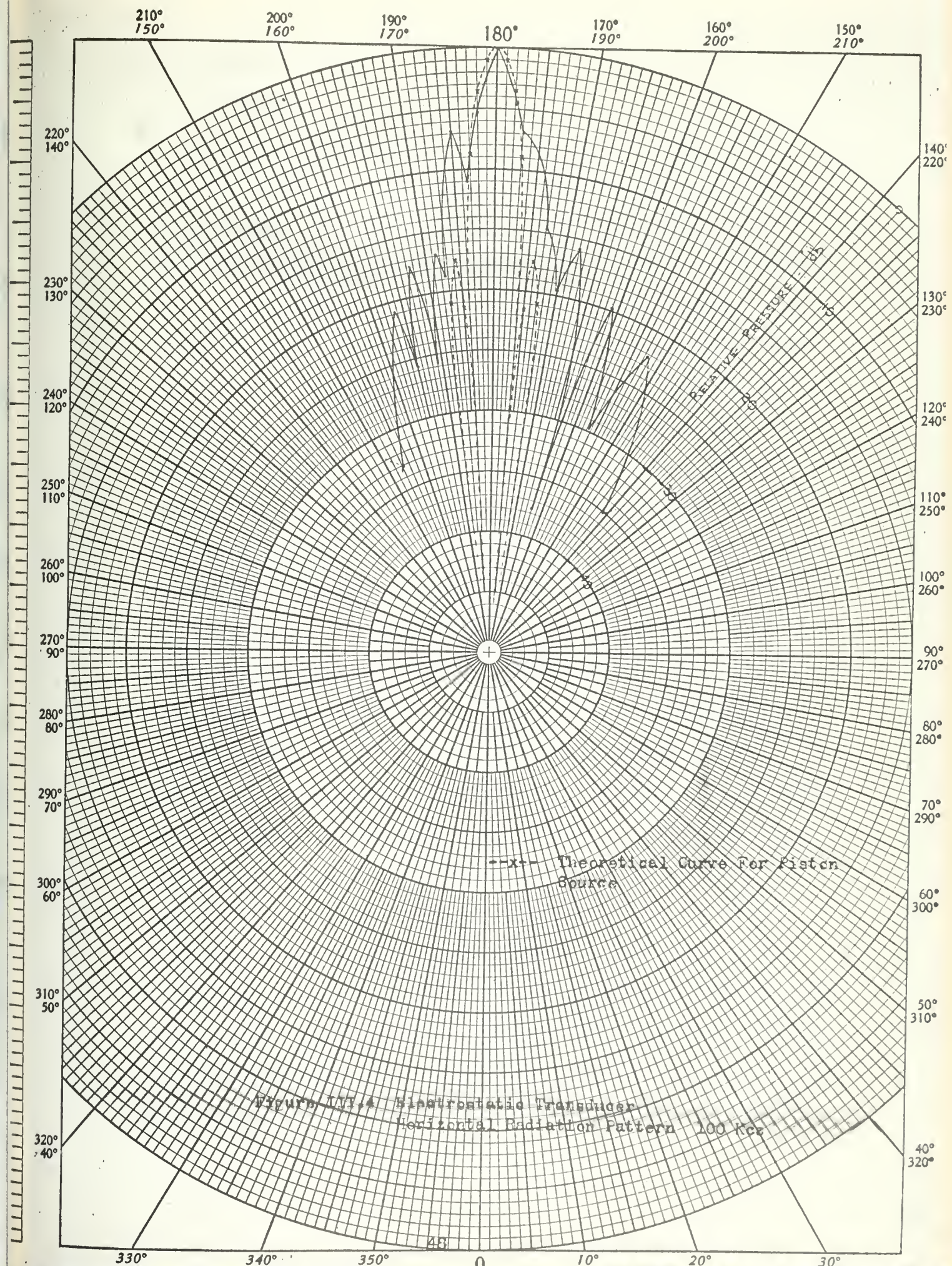

Figure IV.4 Electrostatic Transducer
Horizontal Radiation Pattern 100 Kcs

C. Pulse-Echo System.

1. Design.

Having constructed a suitable transducer, the design of the pulse-echo system was next considered. To limit the bandwidth of the transmitted pulse it was desired to have many cycles of the fundamental frequency within the pulse. Arbitrarily selecting ten cycles as the minimum, a tentative lower operating frequency of 50 kcs determined a minimum pulse length of 0.2 milliseconds. Since the wavelength in water at 50 kcs is approximately three cm, a distance in water of 30 cm is required to contain this pulse. A nominal transducer to reflector spacing of 20 cm was chosen to provide a path length of 40 cm. This provided a volume in the transducer-reflector space of approximately 0.01 m^3. Styrofoam was chosen for the reflector material since its characteristic impedance is nearly that of air and reflection losses should be minimized. A simple framework was constructed to mount the transducer and reflector, with three-point adjustment provided for reflector alignment.

The electronics required for a pulse-echo system consist essentially of a transmitter, a receiver, a display, and a transmit-receive switch. The block diagram of the final system employed in this project is shown in Figure III, 5. The output of the switching network is a pulsed sinusoid with pulse length and repetition frequency determined by the pulse generator. This signal is fed through the power amplifier to the coupling network. Here, the high level signal is applied to the transducer and only a small raction is allowed to pass to the Hewlett-Packard Model 450A amplifier. The weak echo pulses are blocked rom the power amplifier and are fed

through the HP 450A amplifier to the filter and oscilloscope. The filter was used simply in the high-pass setting. Further information on the switching and coupling networks is contained in Appendix III, 1.

2. Initial Observations.

For all measurements the transducer was operated with a polarizing voltage of 200 volts and a driving signal of 20 volts peak value. With a 20 cm transducer-reflector spacing a minimum of 15 echoes were discernible at all frequencies from 50 to 130 kcs, which corresponds to a total path length of six meters. Since the attenuation of sound in fresh water at the highest observed frequency is very small (approximately 4×10^{-3} db per meter) the decrease in echo amplitude with distance in bubble-free water may be attributed primarily to divergence and to reflection loss at the transducer and reflector surfaces. In Figure III, 6 the envelope of the echo amplitudes at 60 kcs is compared with the theoretical curve for a piston source obtained by Seki, et al using the theory of Williams [26,31]. The theoretical curve is the integrated pressure over a plane surface coaxial with the source and of the same area. Assuming that the electrostatic transducer radiates as a piston, for the bubble-free case a comparison of the echo amplitude decrease with the theoretical curve implies that the combined loss for each pair of reflections from the transducer and the reflector is approximately 0.7 db. Close to the source the near field is very complicated and echo amplitudes (echoes 1 and 2) show wide variations which have not been reproduced in Figure III, 6.

The near field effects had been expected but the influence of transducer-reflector parallelism had not been anticipated. Misalignment appears as a modulation of the echo amplitudes which is most noticeable after many reflections and at higher frequencies. This effect has been reported by R. Truell and W. Oates in quartz crystals at frequencies of 70 mcs and above [27]. Alignment of the transducer and reflector by use of the Gauss eyepiece technique resulted in some improvement but the transducer and particularly the reflector surface were not truly plane and the modulation effect could not be completely eliminated. This modulation proved to be a minor factor in the attenuation measurements because differences between echo levels in bubble-free and in bubbly water were used to obtain relative attenuation rather than absolute values. Figure III, 7 shows typical echo patterns as observed on the oscilloscope and illustrates the effect of misalignment.

Sound velocity determination with the pulse-echo system was considered. With an effective acoustic path length of 6 meters and the nominal calibration of the oscilloscope time base, it was estimated that an accuracy of velocity determination of about one percent was obtainable. With the addition of precise time marks more accurate velocity measurements could have been made but since the attenuation measurements were the primary concern, this additional instrumentation was not provided.

3. Attenuation Measurements in Bubbly Fresh Water With the Pulse-Echo System.

It was not intended that this pulse-echo system be capable of absolute attenuation measurements. Over the frequency range of

interest the attenuation of sound in bubble-free sea water varies from 0.001 db per meter at approximately 10 kcs to 0.03 db per meter at 100 kcs. The measurement of attenuation of this order of magnitude would require the use of techniques not particularly suited for use over a wide frequency range in the ocean environment. Relative attenuation may be determined by calibrating the pulse-echo system in bubble-free sea water in the laboratory. These results may then be compared with those obtained when bubbles are introduced into the laboratory sample of sea water or with those obtained in the near surface region of the ocean. The envelope of the echo decay obtained during calibration is caused primarily by divergence, by reflection loss, and by the slight attenuation of the water. Other effects are also present such as that due to misalignment so that calibration data must be obtained at all frequencies of interest. With additional attenuation in the water, such as from air bubbles, the echo voltage levels are each decreased by a term αnd where α is the additional attenuation in db per meter, d is the transducer-reflector spacing in meters, and n is the echo number. By a comparison of each echo with that obtained during calibration the additional attenuation, α , may be determined. Figure III, 6 illustrates a typical fresh water calibration curve and a corresponding curve in bubbly water.

In order to determine the sensitivity of the pulse-echo system it was necessary to have a source for production of microbubbles. It was desired that this source produce bubbles of constant radius and at a controllable rate. Considerable experimentation produced

an electrolysis method which was reasonably satisfactory. Fine platinum or tungsten wires were insulated in glass with the tip of the wire exposed. The tip was then etched to provide a smooth rounded surface. These wires were driven by a negative voltage pulse at a very low repetition rate (from 1 to 2 per second). In general the size was controlled by the pulse amplitude and duration, with a single bubble formed and released by each pulse. By observing bubble rise times it was possible to select those wires that would produce a series of nearly uniform size bubbles with good time stability. In use, a wire would be mounted below the space between the transducer and reflector and a single stream of bubbles would rise through this space.

The bubble radius is determined by observing the speed at which a single bubble rises. Assuming the bubble to be a rigid sphere with constant velocity the Stokes viscous force, $6\pi R\eta v$, may be equated with the buoyant force and the solution for the bubble radius, R, is given by equation (III, 5) where η is the dynamic shear viscosity, v the velocity of ascent, g the acceleration of gravity, and $(\rho_w - \rho_a)$ is the difference in densities of the water and the air of the bubble.

$$R = \sqrt{\frac{9\eta v}{2g(\rho_w - \rho_a)}} \qquad (III,5)$$

This radius may be used to determine the bubble resonant frequency using equation (III, 6). In this equation, γ is the ratio of specific heats, P_o the ambient water pressure, ρ_o the water density, G is a correction for the surface tension, and A modifies the value of γ to take account of heat conduction. The factors G and A are given by Devin [17].

$$f_o = \frac{1}{2\pi R} \sqrt{\frac{3\gamma P_o}{\rho_o} \frac{G}{A}} \qquad \text{(III, 6)}$$

Using the speed at which the bubbles rise and the rate of generation, the average number of bubbles within the transducer-reflector volume may be calculated. Then, assuming no interaction effects, the attenuation α, in db per unit distance caused by a number of bubbles of unique size R is

$$\alpha = 4.34 \ \sigma_e \ N(R) \qquad \text{(III, 7)}$$

where N(R) is the number of bubbles per unit volume and σ_e, given by equation (III, 8), is the extinction cross section for each bubble [8].

$$\sigma_e = \frac{4\pi R^2 \left(\frac{\delta}{kR}\right)}{\left[\left(\frac{\omega_o}{\omega}\right)^2 - 1\right]^2 + \delta^2} \qquad \text{(III, 8)}$$

In equation (III, 8) ω_o is the resonant frequency of bubble size R, ω the frequency of observation, k is 2π divided by the wavelength, and δ the damping constant which has been reviewed by Devin [17]. The actual size of the bubbles within the transucer-reflector volume has a distribution associated with it because 1) the initial bubble size is slightly variable and 2) the bubbles decrease in size during their ascent due to absorption by the water. Observations of the rate of rise over a 15 cm path showed that bubbles of nominal 60 micron radius had variations in size of approximately 5 percent.

A limited amount of bubble attenuation data was obtained in the laboratory with the pulse-echo system. To compare with experimental

attenuation measurements the observed average bubble velocity and the rate of generation were used with equations (III, 5) through (III, 8) to calculate the theoretical attenuation. It was determined that the minimum attenuation measurable with the pulse-echo system was of the order of 0.25 db per meter. At 60 kcs an attenuation of 0.25 db per meter corresponds to a bubble volume concentration of approximately 1.3×10^{-9} assuming bubbles of uniform size. This corresponds to a detectability of roughly one bubble of 52 microns radius in each pint of water. Figure III, 8 compares a set of experimental attenuation measurements with the theoretical curve which was based on an average observed bubble radius of 52 microns, a volume concentration of 5.7×10^{-9} (80 bubbles in transducer-reflector volume), and a damping constant of 0.1. Agreement between the two curves is reasonable, however the theoretical curve is based upon bubbles of uniform size while the actual bubble radii probably deviated no more than 3 percent from the resonant size. It would be expected that the experimental curve would be somewhat broader than the theoretical curve. This would indicate that a slightly different value of damping constant should be used in the theoretical calculations. Sufficient data was not obtained to investigate this further.

An interesting effect observed during attenuation measurements was the shape of the echo-pulse above and below the bubble resonant frequency. At frequencies slightly above resonance the pulse tops were tilted with the amplitude of the leading edge greater than the trailing edge. At frequencies below resonance the reverse was observed. This effect indicated that the transmitted pulse frequency bandwidth

was great enough to cause nonuniform attenuation due to the change of bubble attenuation with frequency. The Fourier transform of a pulsed sinusoid is a (sin x)/x type frequency distribution centered at the fundamental frequency. The width of this distribution to the first zero crossing is 2/T cps and the half-amplitude width is approximately (1.2)/T cps where T is the pulse width in seconds. Thus, the 0.2 millisecond pulse used in this system has a bandwidth of 6 kcs at the half-amplitude points. Since bubble attenuation versus frequency is quite steep the frequency components of the transmitted pulse were indeed being subject to nonuniform attenuation and it is assumed that this is the explanation of the distorted pulse tops.

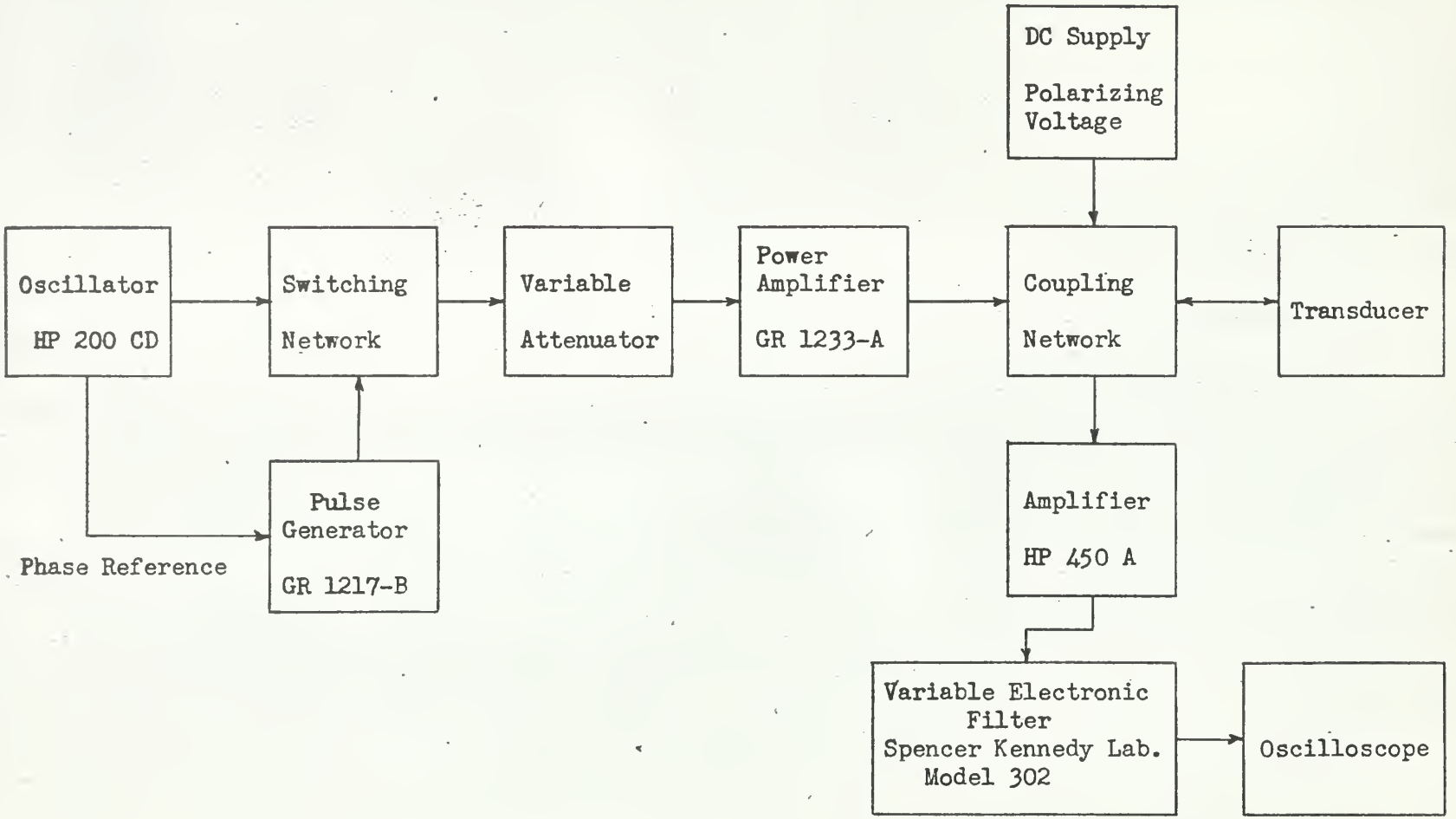

Figure III.5 Pulse-Echo System Block Diagram

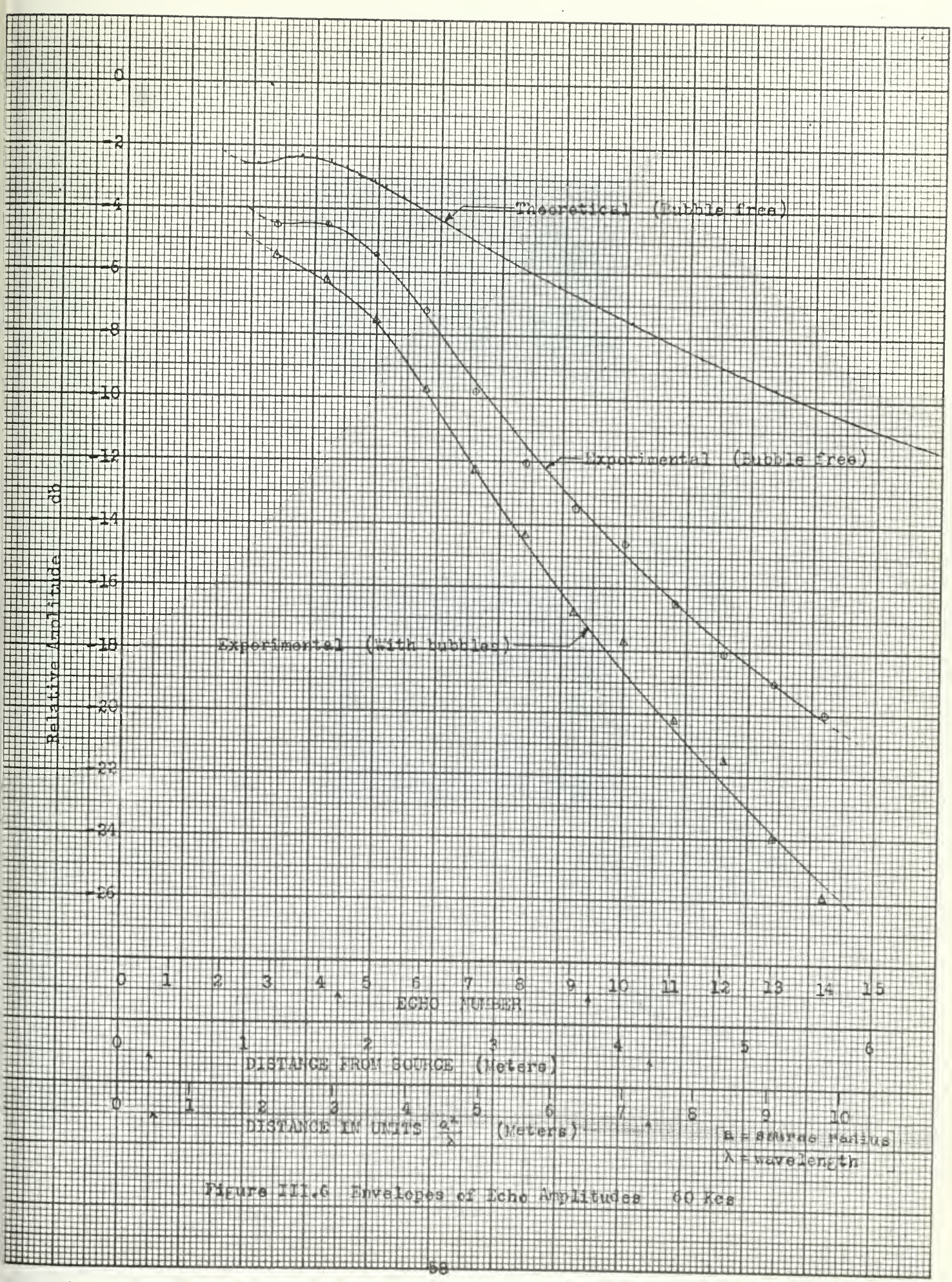

Figure III.6 Envelopes of Echo Amplitudes 60 Kcs

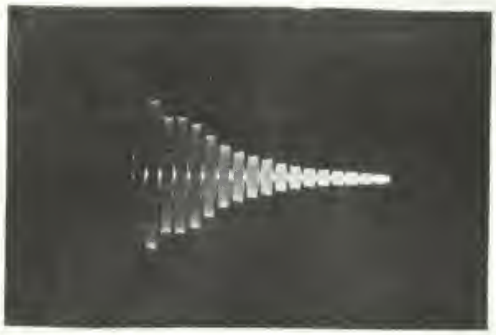

(a) Typical Display at 60 Kcs

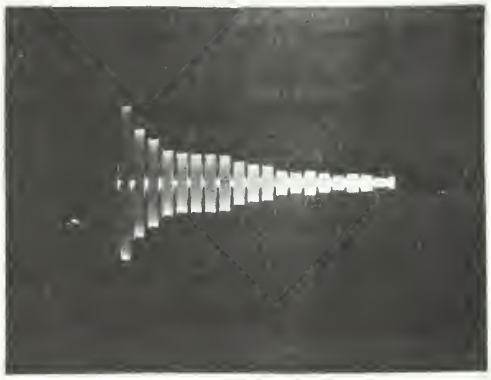

(b) 103 Kcs - Illustrating Modulation Effect
Before Precise Alignment

Figure III.7 Typical Pulse-Echo Displays

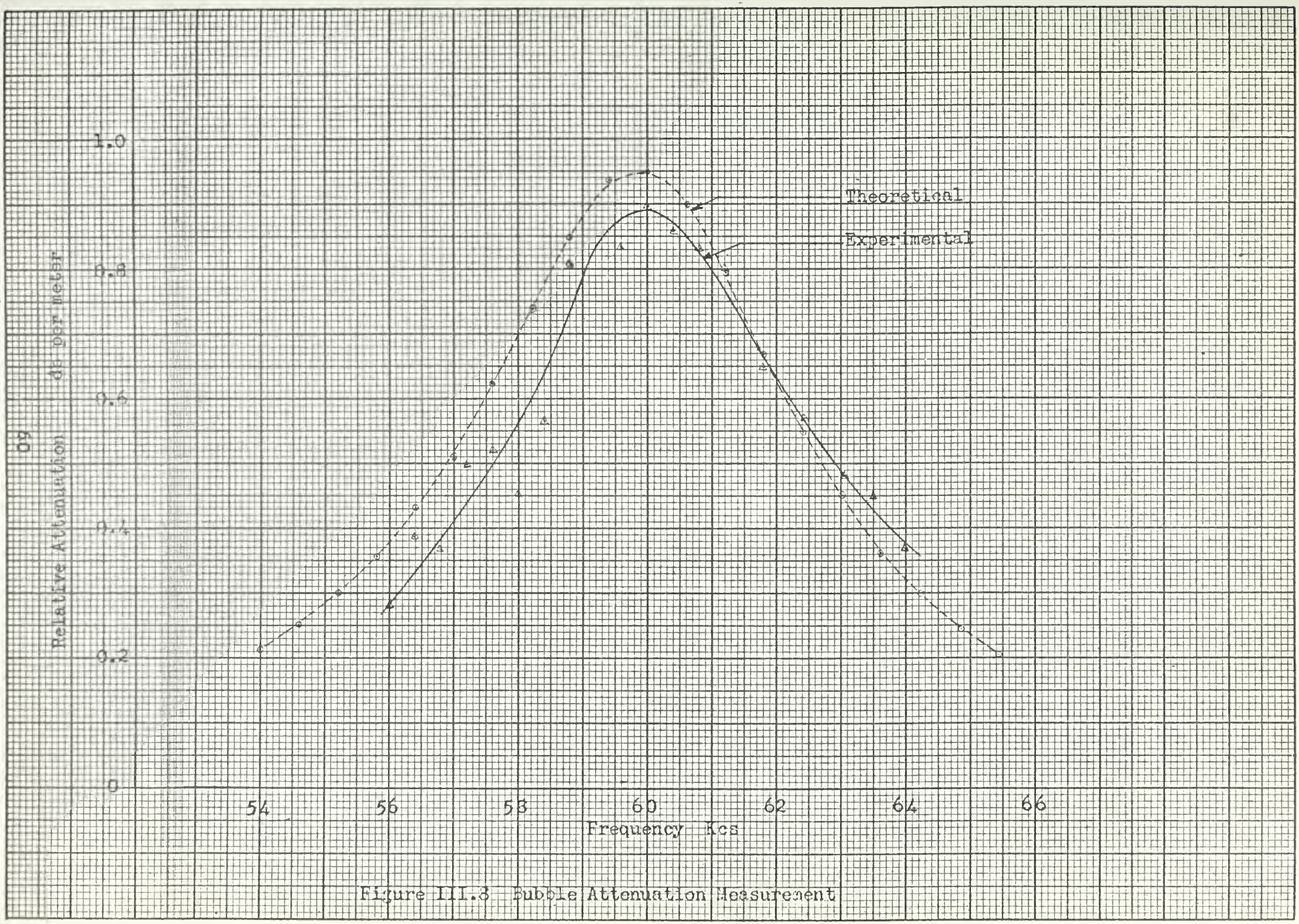

Figure III.3 Bubble Attenuation Measurement

D. Discussion of the Pulse-Echo System.

The electrostatic transducer was found to be well suited for this application which required a relatively large, wide range source-receiver. The pulse response of this transducer was excellent. The pulse-echo system described allows a reasonable volume of water to be examined over the desired frequency range and it can be made rugged enough to withstand shipboard handling. The 0.2 millisecond pulse width selected in this design produced a significant bandwidth which could be reduced by increasing the pulse width. This would necessitate increasing the transducer-reflector spacing to accomodate the pulse. This would also decrease the reflection losses so a longer total path length could be observed although the number of echos received for this length would be decreased. The investigation of frequencies much below 50 kcs will require that this be done as the bandwidth of the 0.2 millisecond pulse becomes a considerable percentage of the fundamental frequency in this region.

Within the ocean persistent bubbles, if they exist, will have a distribution of sizes which is unknown at the present. At any frequency the attenuation due to these bubbles will be the integrated effect of this size distribution and the volume concentration distribution. It is therefore difficult to predict the sensitivity which will be required to adequately determine this effect. Several possibilities exist for improving the sensitivity and accuracy of the pulse-echo system described. Since the additional attenuation effect on echo amplitude increases with distance one method of improving the system is to increase the total path length observable. An increased transducer-

reflector spacing will reduce the losses in the system and operation at a higher polarizing voltage will improve the transducer sensitivity. Both of these will increase the total distance observable. Another area for improvement is in the method of display of the received echoes so that echo amplitudes are determined by a method more accurate than reading from an oscilloscope.

APPENDIX III, 1

PULSE-ECHO SYSTEM SWITCHING AND COUPLING NETWORKS

The switching network was required to provide a pulsed sinusoidal output from a continuous wave source over the frequency range of approximately 20 kcs to 150 kcs. The pulse width was to be variable around a nominal value of 0.2 milliseconds and the repetition rate to be varible around 100 pulses per second. It was further required that no dc level be introduced into the pulse. The circuit used to perform this function is shown in Figure III, 9. This circuit is essentially a diode bridge which is switched by a transistor. In the interval between pulses the pulse generator output is at -40 volts which biases transistor T_1 off and the diodes are non-conducting so there is no output. A positive pulse from the pulse generator causes T_1 to conduct and the signal path is completed thru the diodes and T_1. The introduction of diodes and the transistor in the signal path produces a small amount of crossover distortion in the sinusoidal waveform. To determine the magnitude of this distortion the switching network was biased on and measurements were made at the output of the power amplifier; these were compared to distortion measurements made with the switching network out of the circuit. The switching network increased the second harmonic distortion from 0.2 to 1.5 per cent and the third harmonic from 0.1 to 0.35 per cent, which was deemed to be acceptable. In all other respects the switching network performed satisfactorily.

The coupling network was required to perform three functions;

couple the polarization voltage to the transducer, limit the signal applied to the receiving amplifier during transmission to prevent overloading, and disconnect the power amplifier during the receive period to prevent the noise in its output from obscuring the echoes. The circuits comprising the coupling network are shown in Figure III, 10. These elements were chosen as being the simplest capable of performing the required functions. The diodes in module 1 are essentially a short circuit to the high level transmitted signal but present a resistance of greater than 250 K ohms to signals of 100 millivolts rms or less. The slight amount of distortion introduced in the transmitted signal by these diodes, however, is included in the data given in the previous paragraph. Module 3 utilizes similar diodes to short the receiver input during transmission and then present a high resistance to the low level echo signals. Module 3 is a simple R-C circuit to apply the polarization voltage to the transducer.

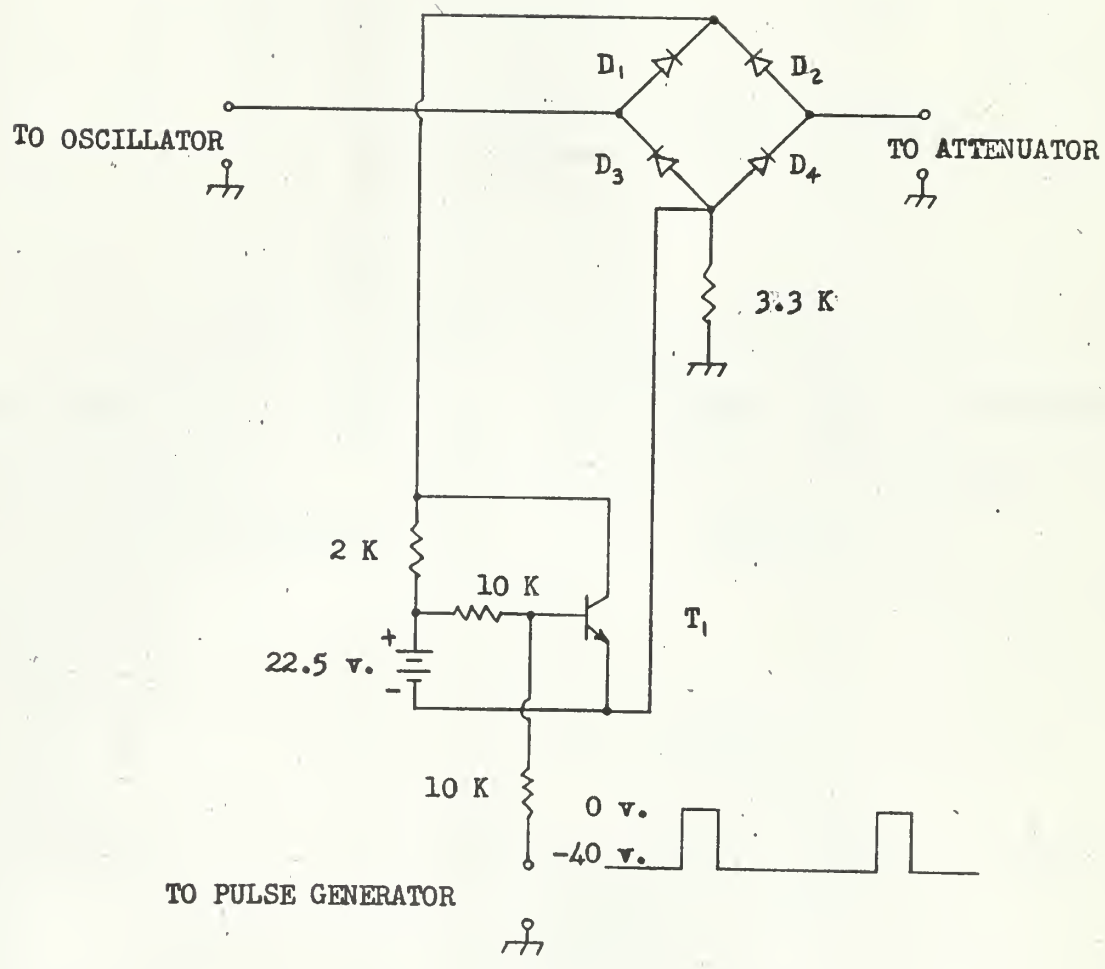

$D_1 - D_4$ - 1N 645
T_1 - 2N 1310

Figure III.9 Switching Network

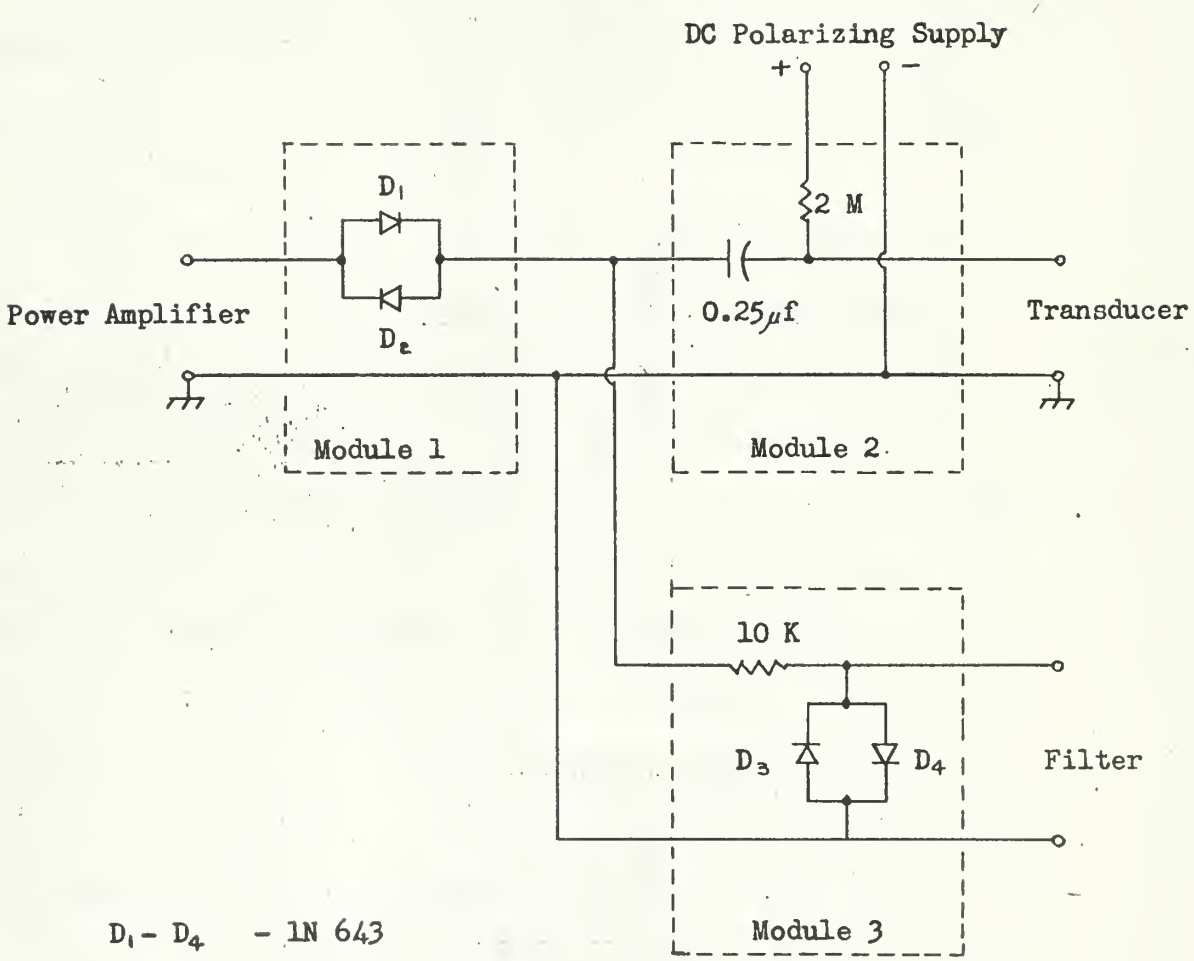

Figure III.10 Coupling Network

IV

BUBBLE PHOTOGRAPHY

A. Introduction.

A survey of the literature reveals little material pertinent to micro-bubble photography. Attempts at bubble photography are mentioned in only two studies of acoustic scattering by bubbles. A brief summary of the methods described in those articles follows:

1. Fox, Curley, and Larson[18].

In a laboratory experiment primarily directed towards measurement of phase velocity and absorption of sound in very bubbly water, the authors determined from photographs the actual bubble distribution inside a small tank. The bubbles were illuminated by back lighting using an electronic flash. A fine wire was placed in the field of focus to provide a reference for determination of bubble size from the negatives. The lens system used gave a magnification of seven, and enlarged prints enabled a final overall magnification of 30. The bubble density in the water was considerable; on the order of 2×10^{-4} c.c. air per c.c. water.

2. Glotov, Golobaev, and Neuimin[19].

In this recent laboratory experiment, bubbles were generated in a rather small tank (2x2x3 meters) by artificially produced wind and wave action. The bubbles thus produced were trapped in a device called a "bubble catcher." This piece of equipment consisted of a hollow cylinder, the top and bottom of which could be sealed simultaneously thus entrapping the bubbles. The upper seal was glass, and the bubbles after rising the settling on the

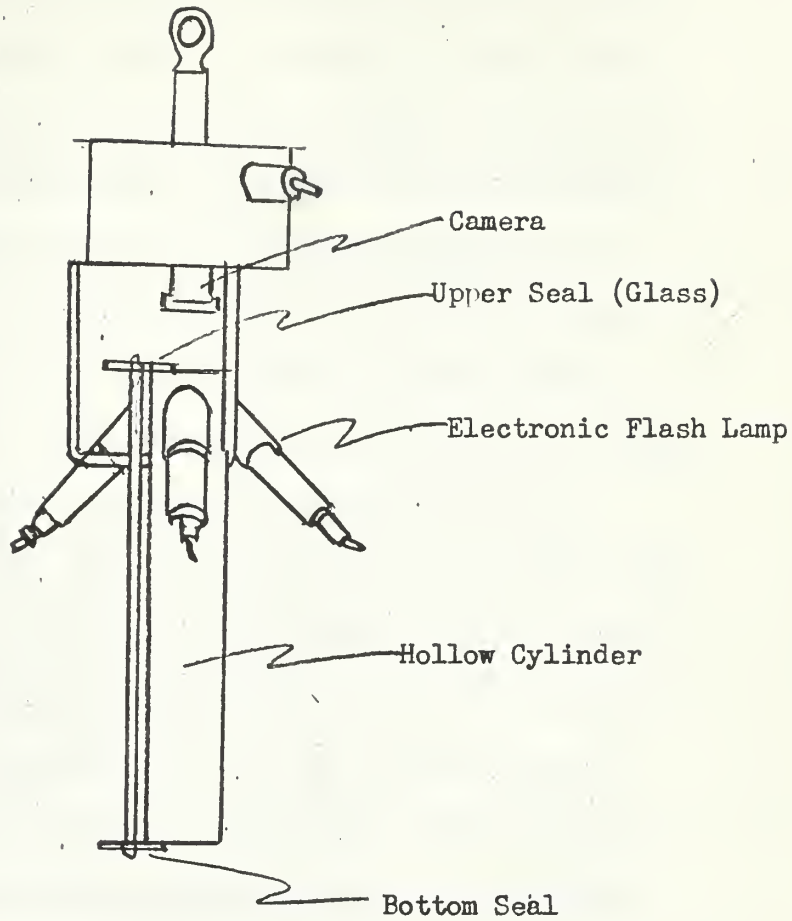

Figure IV-1. Schematic of "Bubble Catcher"

bottom of this seal, were photographed through the glass. Illumination for the photographic process was provided by three lamps at 120° intervals and canted 45° to the rear as shown in Figure IV-1. It was stated that this arrangement "provided the best conditions for observing the bubbles" and "the use of these lamps made it possible to distinguish the bubbles from solid particles and to measure the particle size reliably." Photographs were made 1:1.

Two recent articles written in connection with nuclear bubble-chamber photography, proved to be of aid in establishing and verifying the photographic procedures used in this project[16,30]. The article by Welford was of particular value. Although published after our work in bubble photography had begun, it served to reenforce many of the procedures which we had already adopted.

Because the literature available had at best only marginal applicability to the problem of getting photographs of bubbles at sea, it was decided to develop methods of photography idependently. Some of the problems encountered, attempted solutions, and reasons therefor are mentioned and the final assembly is described in the following paragraphs.

B. Development of Photographic Techniques.

1. Introduction.

In order to establish or disprove the existance of bubbles in sea water, it is essential that the largest possible volume of water be pictured in each photograph. In this manner, a statistically valid sample of water is obtained with the fewest photographs. Since nothing was known of the concentration of these bubbles in situ, a certain degree of arbitrariness was involved in the construction of the camera system.

There are three closely inter-related variables which are common to any photographic system: lighting (including shutter speed), optics (depth of field, degree of magnification, lens system, etc.), and the type of film.

The lighting must be sufficiently intense to permit apertures small enough to provide a reasonably large depth of field and/or permit use of finer grain film. Shutter speed in this project was not a factor because an electronic flash with a maximum pulse length of 4 milliseconds was used -- fast enough to freeze any motion of bubbles or camera.

The degree of magnification must be great enough to permit detection of bubbles down to a small size, say 10 microns radius, yet not so great that an excessively small depth of field results.

Finally, the film speed must be as fast as possible, thus permitting the use of smaller apertures or less intense lighting, and yet have sufficiently fine grain to allow bubbles to be distinguished from other matter that might be present in the water.

To enable a large volume of water to be photographed, a large negative is also desirable.

The camera system finally constructed, therefore, was considered the best compromise among these variables. The various steps involved in arriving at the final configuration are outlined in the following paragraphs.

2. Lighting.

a. Angle of Illumination.

Trials were made using several different angles of illumination; however, back lighting was not attempted. Any method of providing back lighting entails certain difficulties which will be mentioned in subparagraph 3. below. The angle of illumination was varied from a position at right angles to the camera lens axis to a back angle of about 120°. Somewhat surprisingly, the angle of illumination within these limits had a negligible effect on the ability to discern the presence of bubbles from the negative. In the final installation, illumination at right angles to the camera lens axis was used.

It was also established that the use of more than one light was indeed helpful in distinguishing bubbles from other particles. The final installation consisted of two electronic flash units spaced 120° apart in a plane perpindicular to the camera lens axis. This spacing was chosen in the hope that the periphery of the bubbles would be illuminated thus enabling them to be easily distinguished from non-spherical particles present in the water.

b. Type of Light.

Several different light sources were tried in the hope that a source of continuous light would be adequate for photographs. However, the strong attenuation of light in water and the motion of the bubbles made the use of a flash essential. An electronic flash was constructed for use in the final installation.

Because of the difficulty of determining the correlation between flash bulbs and electronic flash units, several pictures were taken using a borrowed electronic flash in the experimental setup. On the basis of these trials, it was decided that electronic flash units capable of 200 watt-seconds output would provide sufficient illumination in the final installation.

c. Filtering.

The use of a red filter during the picture taking was found to be an aid in bubble recognition; however, lack of time and a suitable material for use in the final installation precluded full investigation of filtering techniques.

3. Optics.

The major difficulty encountered during picture taking in the experimental setup was the scattering of light by bubbles illuminated outside the field of focus. A sample of such a photograph is shown in Figure IV-2(a), and although admittedly an extreme case, it is obvious that reliable determination of bubble size from such a photograph is impossible.

To be photographed accurately, bubbles must be in the region of sharp focus of the camera. Furthermore, only the field of focus can be illuminated, also pictures as in Figure IV-2(a) result.

Figure IV-2(a). Photograph Showing the Effect of Scattering Caused by the Illumination of Bubbles Outside the Field of Focus.

Figure IV-2(b). Bubble Photograph Taken Using Collimated Light Under Conditions Otherwise Identical to Those of IV-2(a) Above.

As mentioned earlier, any methods of back lighting would require that bubbles in areas outside the field of focus but still in the field of the lens be excluded. One possible method, sketched in Figure IV-3, would be to exclude water and bubbles from regions not in focus by putting glass, air or other transparent material in these regions, thus permitting water and bubbles only in the field of focus. This method is satisfactory for laboratory experiments, but not for use at sea. At sea, turbulance caused by the movement of camera, boat, and water would tend to generate and trap bubbles within the field of focus of this system, so this approach was abandoned.

In the method finally used, the light from the flash sources was collimated to illuminate only a shallow plane at right angles to the camera lens axis at the focal position. The system is sketched in Figure IV-4, and a photograph showing the improvement resulting from its use in an early trial appears in Figure IV-2(b). The principal drawback to this procedure is the reduction in the intensity of illumination because of the collimator. After several adjustments, this technique provided satisfactory pictures.

4. Film.

Initial attempts at bubble photographs were made using polaroid film of various types. Unfortunately, with the possible exception of the very expensive Type 53 film, it was learned that Polaroid films all contain pinholes to a greater or lesser degree. These pinholes are roughly the size of the images of bubbles

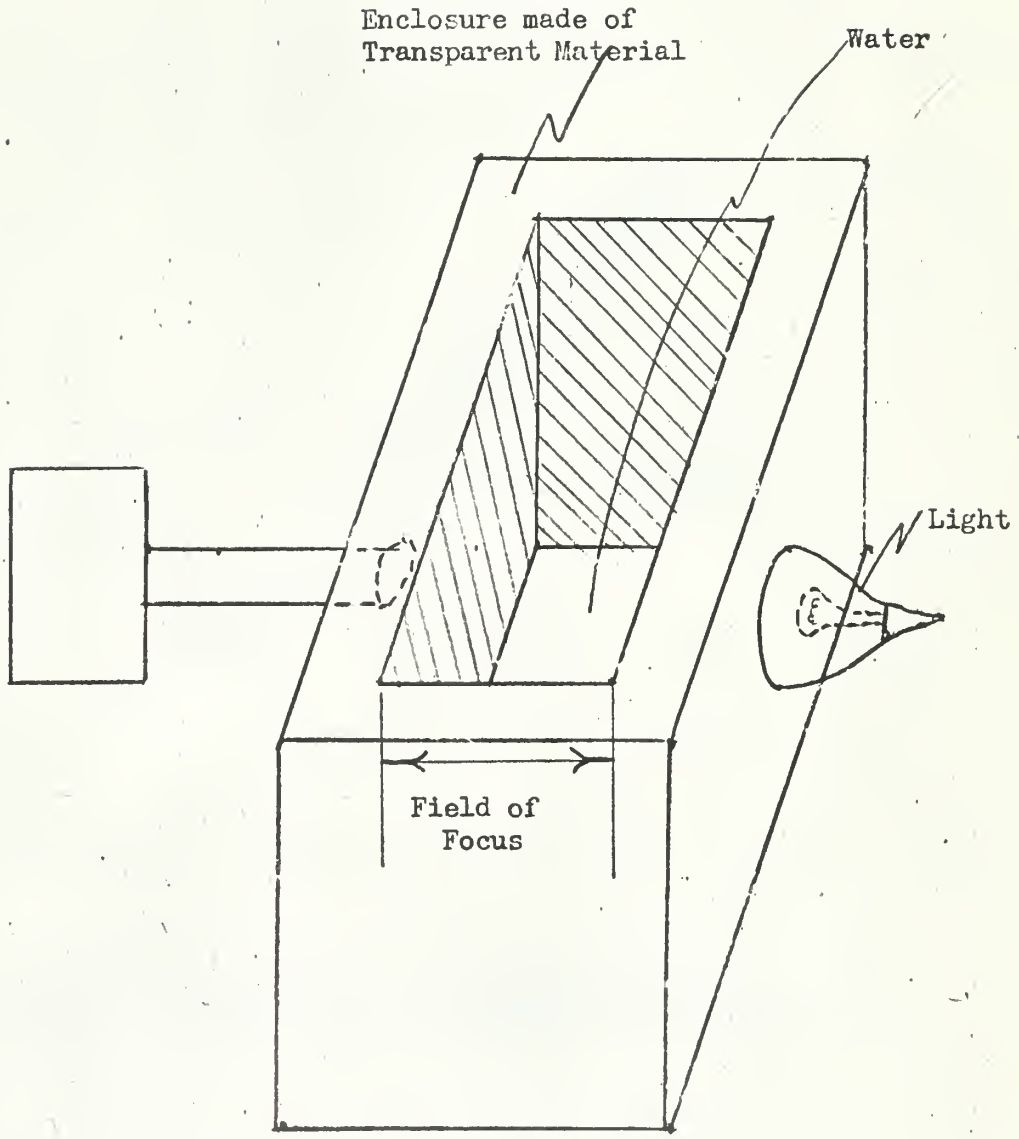

Figure IV-3. Example of a Photographic System using Back Lighting.

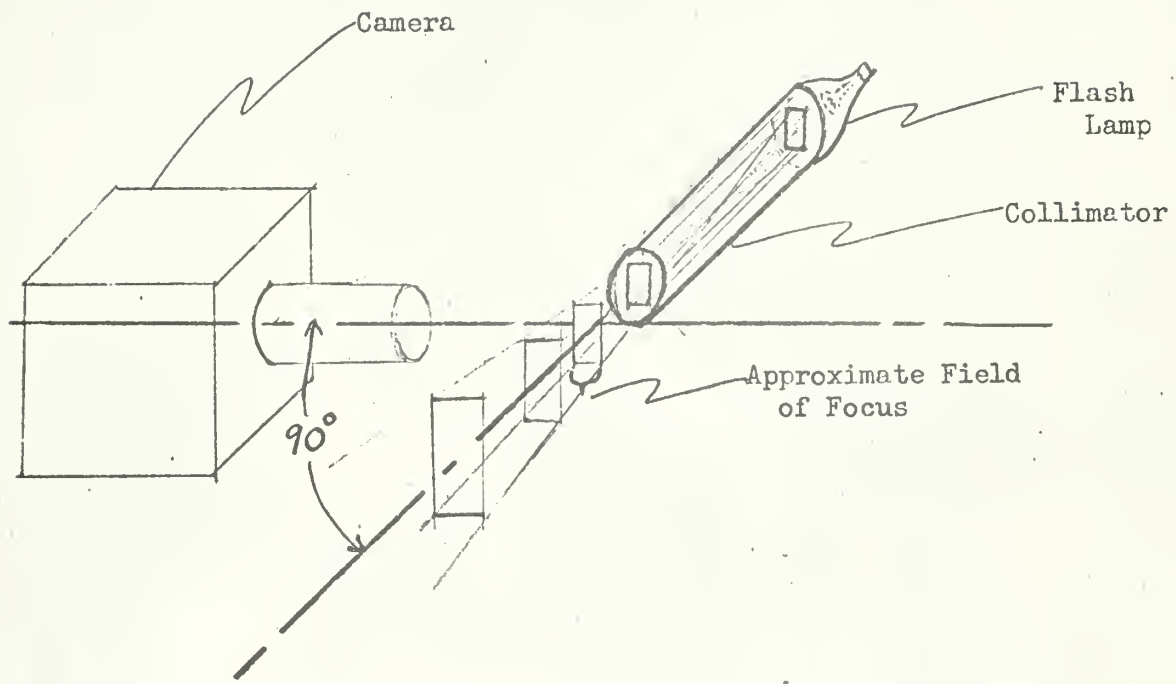

Figure IV-4. System of illumination using collimated light. In the actual installation two collimators were used which illuminated a field of focus $\frac{1}{2}$ cm deep.

commonly found in water and indistinguishable from them on the film. Kodak Royal Pan and Tri-X films were subsequently used with good results. Both proved sufficiently fine grained to allow considerable magnification of the negative. In the final installation Kodak Tri-X and the very high speed, coarse grain Royal-X films were used.

C. Final Camera Installation.

1. General.

From the information contained in available literature about microbubble persistence, it was decided to attempt photography of bubbles down to a radius, a, of 10 microns. Geometric optics still apply at this size since for the longest wavelength (red) light, Ka=105 [16].

Because of the limited depth of field, the volume of water to be photographed in each picture was very small; therefore, a negative size as large as practicable was desirable. Pictures were to be taken to a depth of 50 feet, so automatic control of camera functions was also essential.

An automatic 70mm aerial camera was obtained and modified to provide magnificatior and synchronization with the electronic flash. The focal plane shutter was removed and a solenoid-actuated, between-the-lens shutter was installed. The final installation is shown in Figure IV-5.

2. Lighting.

Two collimated electronic flash units were constructed and adjusted to illuminate a $\frac{1}{2}$cm depth of field. The completed units are shown in the accompanying photographs (Figure IV-5), and the electronic circuit diagram is shown in Figure IV-6.

3. Enclosure.

An aluminum camera enclosure was constructed as shown in Figure IV-5. The enclosure was of a size adequate to permit attachment of a bellows to the camera in order to obtain varying

APR 1964

Side View of Watertight Enclosure

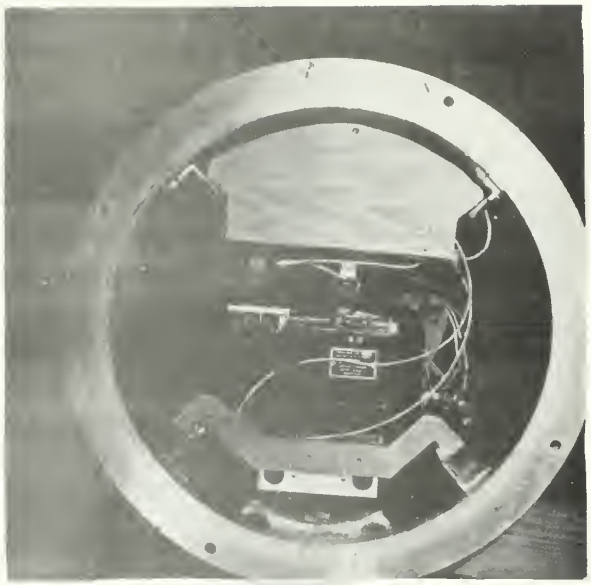

APR 1964

Rear Access Opening. Camera and Mount are on the Bottom. The Wooden Box Contains the Electronic Circuits and Storage Capacitors.

APR 1964

Front View Showing the Cable Access, Two Collimator Assemblies Mounted at 120°, and Lens Port.

APR 1964

Front View Closeup. Note the Collimator Slit in the Right Hand Assembly.

Figure IV-5. Photographs of the Completed Camera Assembly

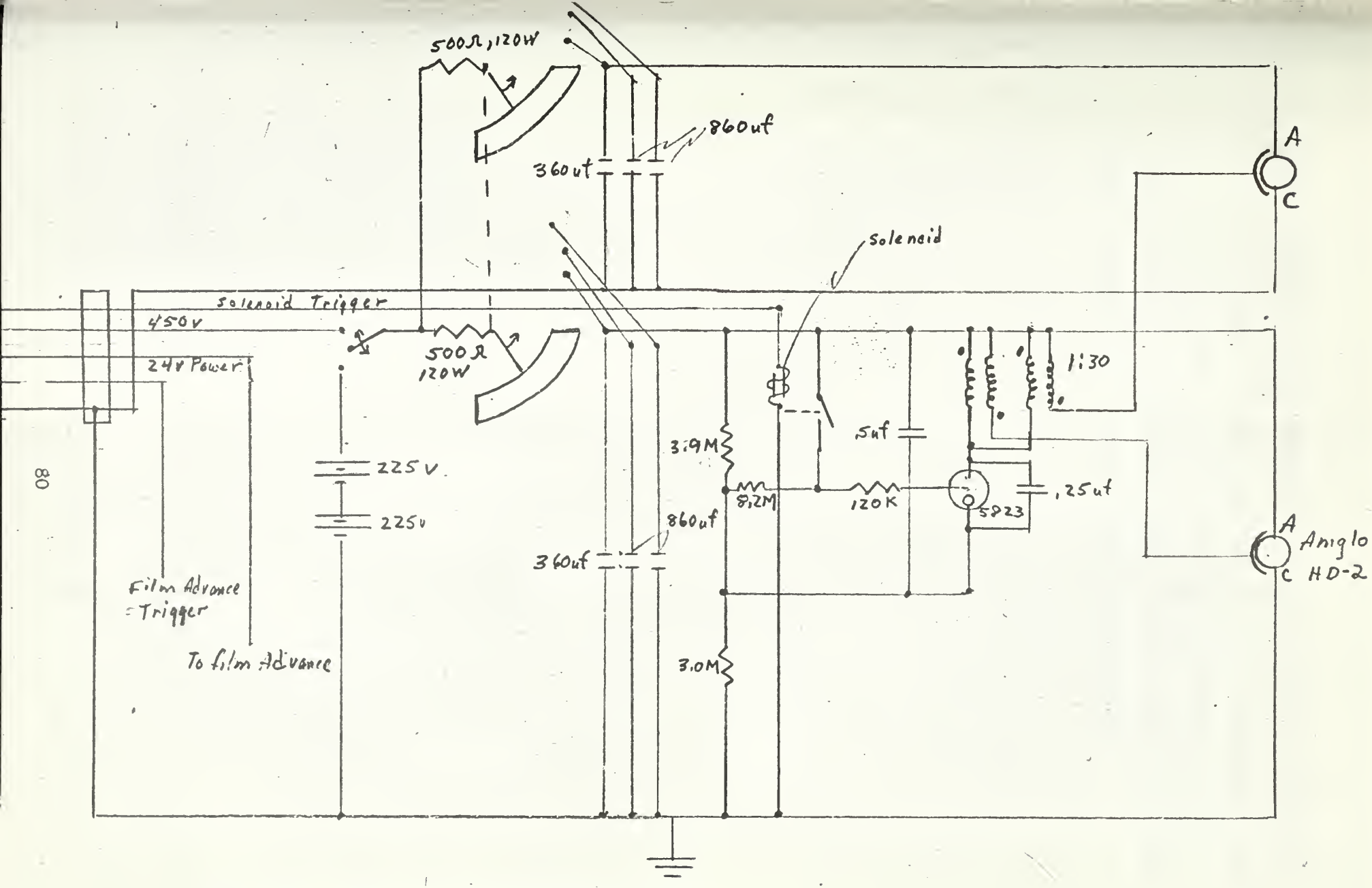

Figure IV-6. Electronic Flash Circuit Diagram.

degrees of magnification between 1:1 and 4:1. The final enclosure was 16" in diameter, 36" long, and with the camera installed, weighed 130 lbs in air. Because of its relatively light weight and large displacement, it was necessary to strap 150 lbs of lead to the outside of the enclosure in order to make it sink in water.

D. Results.

1. Procedure

a. Laboratory Checkout.

(1) Equipment.

The camera was first set up to take pictures which would give a magnification of 4:1. Although the total volume viewed at this maximum value of magnification was only 1 c.c. (Picture area = 1.96 cm^2 x $\frac{1}{2}$ cm depth of field), this value was selected in order to determine the minimum bubble size which could be photographed.

The primary difficulty experienced with the equipment occured with the electronic flash tubes. These devices are evidently very sensitive to overload. This fact coupled with the heat generated by the tube in the small enclosure caused the burn-out of several tubes. Although rated at 200 watt-seconds, it was found that the maximum energy actually possible was in the vicinity of 150 watt-seconds.

(2) Photographic interpertation.

Some surprising effects were discovered in the first bubble photographs taken with the completed camera system. It was found that the collimated flash beams, rather than illuminating the entire periphery of the bubbles as had been anticipated, reflected off of the bubbles exactly as parallel light would off of a reflecting spherical surface, i.e. two spot reflections, one from each flash on each side of the bubble. This fact is demonstrated in Figures IV-7 and IV-8. However, in these photographs the outlines of both the ball and the bubbles are visible

Figure IV-7. Photograph of Bubbles Suspended on the Edge of a Ruler. Markings are 1 mm Apart.

Figure IV-8. Photograph of a 490 micron Steel Ball, and Glass Beads Suspended in Water

because the material on which the ball and the bubbles are suspended broke up the collimated beam, causing the entire periphery of the objects to be illuminated as well as the predominant spots.

Figure IV-9 is a picture of bubbles (generated by electrolysis and allowed to rise through the field of focus) taken without any objects nearby which would tend to make the flash diffuse. The radius of these bubbles can be determined by measuring the distance between the spot reflections.

Figure IV-9(a) shows the geometry of these spot reflections and the method by which the bubble radius may be calculated, i.e. radius = 0.81 x distance between the center of the two reflections.
In this figure the collimated light from the electronic flash is shown incident in a plane perpendicular to the x axis at an angle of 30° from the horizontal. That incident light which is reflected through 90° and parallel to the x axis enters the camera. The incident ray, the normal to the sphere at the point of contact, and the reflected ray parallel the x axis all lie in the same plane with the angular relationships as shown.

The "spots" have a finite width as seen in Figures IV-7,8, and 9, and their size is dependent on both bubble size and the sharpness of focus. This size variation makes measurements using the edges or extremities of the "dots" variable, therefore, consistant readings can only be obtained by measuring the distance from the estimated center of one dot to the center of the other. A micrometer slide was used to obtain readings of the distance between the dots directly from the negatives. The instrument has graduations in 10 micron intervals, and lengths may be estimated to approximately one micron.

Figure IV-9. Photograph of a stream of Bubbles Generated by Electrolysis. The Reflections from Those Bubbles in Focus Show as Two "Dots" or "Spots."

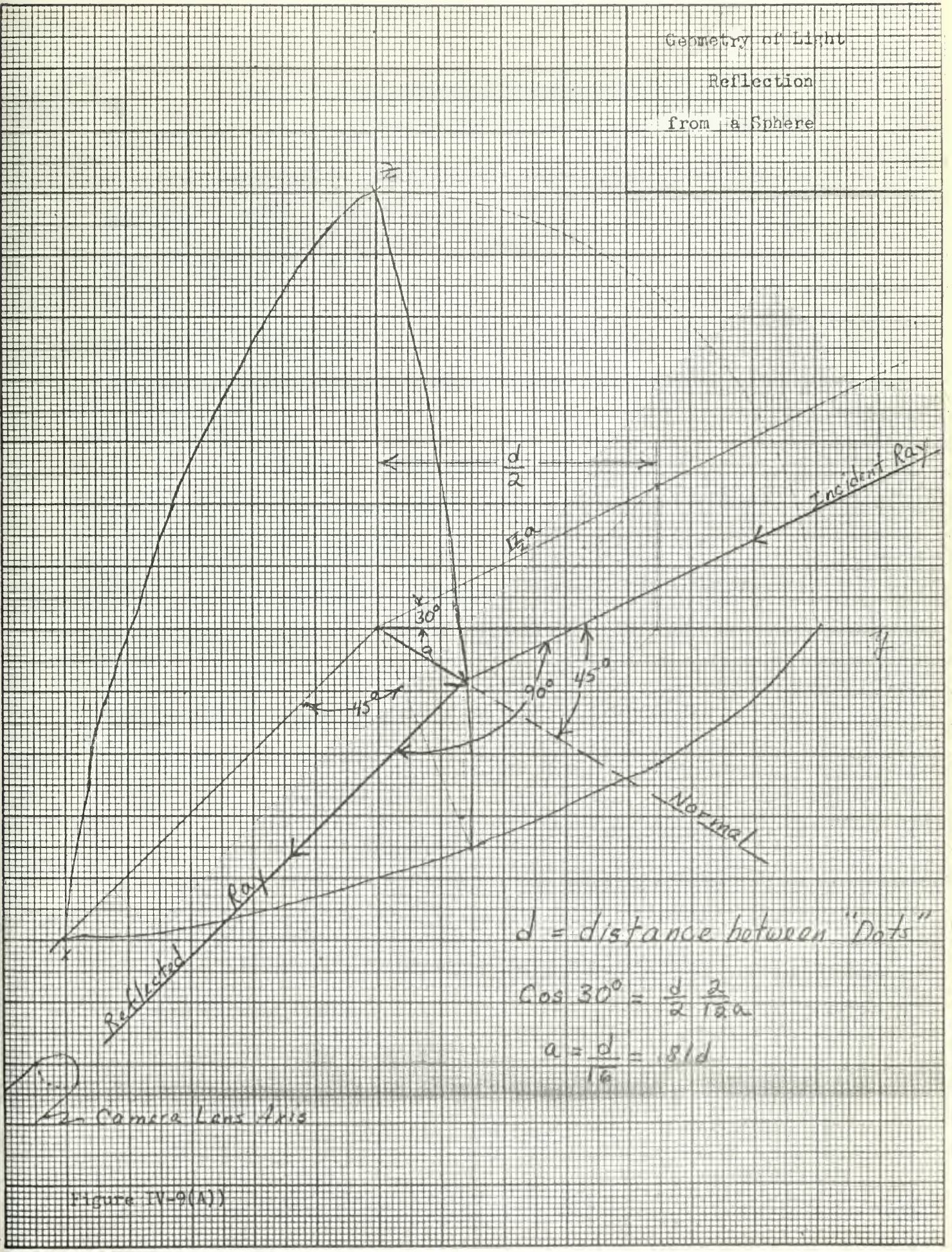
Geometry of Light
Reflection
from a Sphere
d/2
Incident Ray
30°
a
45°
90°
45°
Normal
Reflected Ray
d = distance between "Dots"
Cos 30° = d/2 · 2/√2 a
a = d/16 = .81d
= Camera Lens Axis

Figure IV-9(A))

A check on the accuracy of the technique was made by photographing a steel ball and several glass beads suspended in water. The diameters of these spheres were then computed from measurements taken on the photographic negatives, and compared with those obtained by measuring the spheres with a micrometer calipers. Because the center of the "dots" must be estimated, successive measurements from the photograph of any single sphere varied slightly; therefore, several measurements were made on each sphere and then averaged.

A diameter of 992 microns for the steel ball was obtained by averaging measurements from the photograph of Figure IV-8. This value is within 1.3 per cent of the diameter of 980 microns obtained using the micrometer. No single photographic measurement exceeded the value of 980 microns by more than 3 per cent. Similar comparisons between photographic and micrometer measurements were made on glass beads down to a radius of approximately 100 microns, and all such comparisons were within 5 per cent of one-another.

With the camera adjusted to give 4:1 magnification and using Tri-X film, the distance between "dots" was measurable on bubbles with a radius as small as 20 microns. The lower limit is reached because of the tendancy of the "dots" to merge on bubbles of small radius.

b. Dockside Checkout.

After the laboratory adjustments had been satisfactorily concluded, several sequences of pictures were taken at dockside.

Water conditions in general were very clear, and in the early pictures the sunlight caused considerable darkening of the negatives. Although these negatives were still transparent, much of the contrast was lost. Failure to recognize this factor caused us to reduce the degree of magnification in order to increase the volume of water photographed. In view of the great concentration of objects later observed on high-contrast negatives taken under similar circumstances (but with a shield to exclude sunlight), this action was possibly too hasty and should be reevaluated if high particle concentration are found to be general.

A final series of photographs were taken in the Monterey Marina over the side of the Postgraduate School Oceanographic boat. Both Tri-X and Royal-X films were used with an aperture setting of f8. Pictures were taken at the surface and 10 feet; the water was flat, calm and very clear. The photographs shown in Figures IV-10 and IV-11 were obtained, although some darkening of the negative was again experienced because of the sunlight despite the light shield. The most interesting pictures appeared on the Royal-X film. Evidently insufficient flash light was available to register the smaller images on the slower speed Tri-X; however, larger objects did register on this film.

The pictures obtained on this run were then projected to give an overall magnification of 100:1. The size of the objects which appeared as dark images on the negatives were measured directly from the screen. Unfortunately, there was no positive way of determining whether or not the objects below a size of 50-60 micron radius

Figure IV-10. Photograph of Surface Water, Monterey Marina.

Figure IV-11. Photograph of Water at Depth 10 Feet, Monterey Marina.

were bubbles. The graphs of the distribution of particle size shown in Figure IV-12, therefore, are for interest only, and no conclusions should be drawn from them.

Because of time limitations and the extreme difficulty in obtaining the services of riggers and a crane, no further pictures were attempted at sea.

2. Summary.

The bubble photography system developed is capable of providing measurable photographs of bubbles with a radius as small as 20 microns, when Tri-X film and a 4:1 magnification are used. With the same magnification, measurement of bubble size from the photographs can provide readings within 3 per cent of the actual values for bubbles of approximately 500 micron radius, and within 5 per cent for bubbles down to a radius of approximately 100 microns. The system is suitable for use in calibrating and checking acoustic methods of measurement.

Pictures taken in the Monterey Marina have shown that bubbles down to a radius of 50-60 microns exist in sea water, and in considerable numbers close in shore.

These early trials have shown that the performance of the photographic system has been hampered by insufficient light from the electronic flash system. The experience gained during these trials however, has shown ways in which the lighting may be improved, and these suggestions are contained in paragraph 3. which follows.

3. Recommendations.

The primary purpose of the recommendations is to increase the

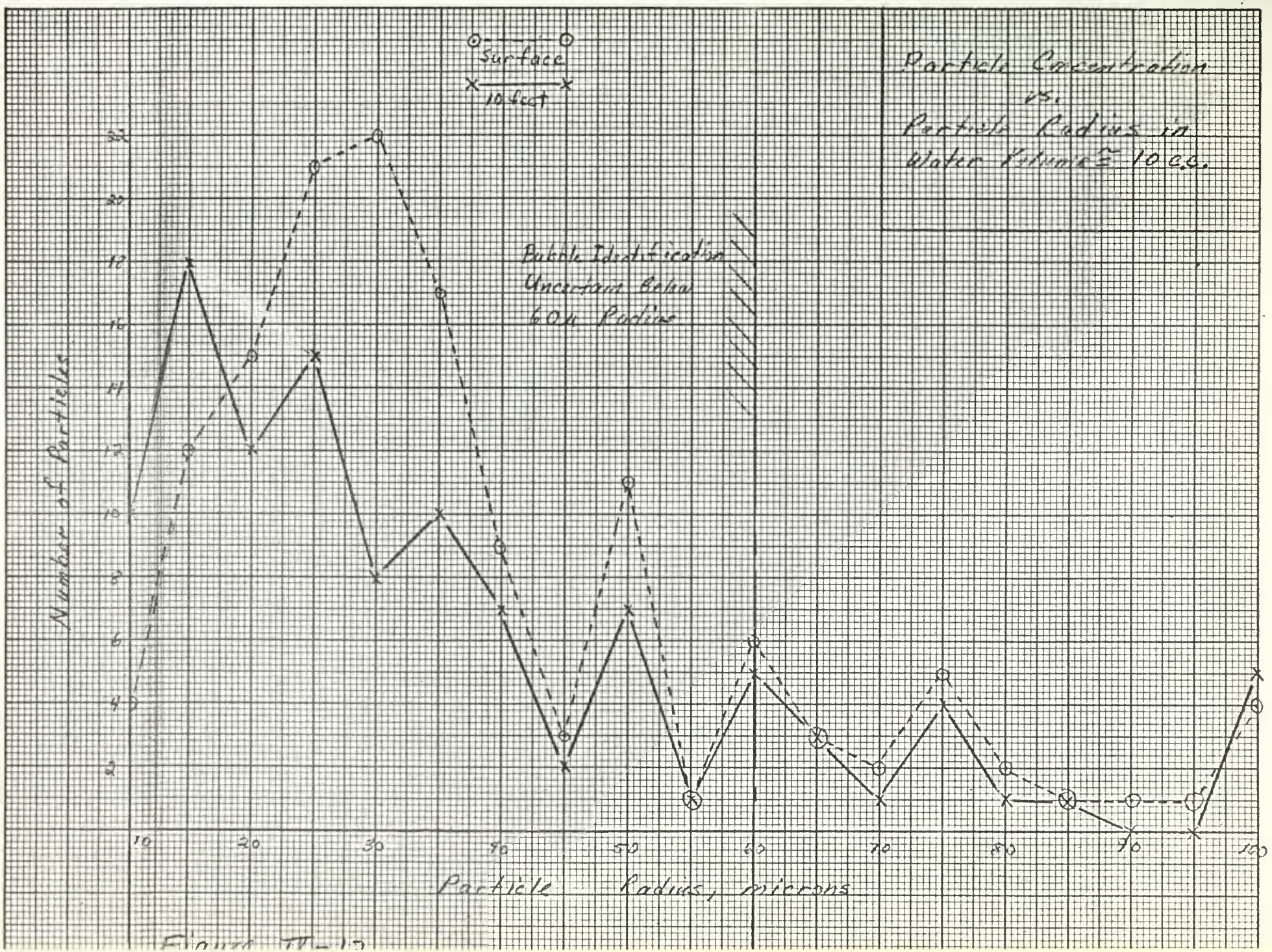
Surface
10 feet
Particle Concentration
vs.
Particle Radius in
Water Volume = 10 c.c.
Bubble Identification
Uncertain Below
60 μ Radius
Number of Particles
Particle Radius, microns
10
20
30
40
50
60
70
80
90
100
2
4
6
8
10
12
14
16
18
20
22

Figure IV-12

intensity of the collimated electronic flash received by the camera after reflection off bubbles. With the relatively large lens opening necessary (f5.6) when using the slower speed Tri-X film, some scattering of the light from objects slightly out of focus still occurs. Increased light intensity will permit a smaller aperture, increase the depth of field, and thus permit use of the finer grain, Tri-X film. Suggested methods of increasing the flash intensity follow:

a. Some improvement may be easily obtained by moving the collimators closer to the camera lens axis, and by moving the lens port of the enclosure closer to the plane illuminated by the collimated beam, thus decreasing the distance the light must travel through the water. In average coastal water conditions, these modifications should provide roughly a 20 per cent increase in light intensity.

b. The intensity of the electronic flash may be improved by experimenting with different capacitor combinations and operating voltages until the maximum safe operating values are determined. A shortage, since alleviated, of electronic flash tubes precluded complete trials when the flash units were initially tested.

c. Should the above techniques fail to provide the necessary increase in illumination, the only alternative is to construct an electronic flash unit capable of greater output, despite the increase in complexity such a unit will entail. A relatively simple way of increasing the power output could be accomplished by construction of a 1000 volt system, and by connection of the

capacitors presently in use in series to withstand the increased voltage. An AMGLO HD-3 or similar flash tube could be used in such a system and mounted in the present collimator assemblies without mofidication.

V

BIBLIOGRAPHY

1. Alber, V. M. Underwater Acoustics Handbook. The Pennsylvania State University Press, 1960.

2. Beranek, L. L. Acoustic Measurements. Wiley and Sons Inc., 1949.

3. Dorsey, N. E. Properties of Ordinary Water Substance. Reinhold Publishing Corporation, 1940.

4. Heuter, T. F. and Bolt, R. H. Sonics. Wiley and Sons Inc., 1955.

5. Horton, J. W. Fundamentals of Sonar. U. S. Naval Institute, 1957.

6. Kinsler, L. E. and Frey, A. R. Fundamentals of Acoustics, 2nd Edition, Wiley and Sons Inc, 1962.

7. Oceanography (edited by M. Sears). Publication No. 67, American Association for the Advancement of Science, 1961.

8. Physics of Sound in the Sea. Division 6, Vol. 8,NDRC Summary Technical Reports.

9. Vigoureaux, P. Ultrasonics. Wiley and Sons Inc., 1951.

10. Naval Electronics Laboratory. Do Invisible Bubbles Exist in in the Sea?, by E. C. LaFond and R. F. Dill, Technical Memorandum TM-259, September 1957.

11. St. Anthony Falls Hydraulic Laboratory, University of Minnesota. An Acoustic Study of Gaseous Micro-bubbles in Boundary Layers and Propeller Wakes, by J. F. Ripken and J. M. Killen. December 1962. Rept. no. 67.

12. Vitro Laboratories. Microbubble Persistance (A Preliminary Research Report), by W. R. Turner. January 1960. Tech.Note TN-N4329-12960.

13. Vitro Laboratories. Precision Ultrasonic Measurements for Microbubble Research, by W. R. Turner. July 1963. Tech. Note 01654.01-1.

14. Vitro Laboratories. Physics of Microbubbles, by W. R. Turner. August 1963. Tech Note 01654.01-2.

15. Chapman, R. P. and Harris, J. H. Surface Backscattering Strengths Measured with Explosive Sound Sources. Journal of the Acoustical Society of America (JASA), v. 34, no. 10, October 1962: 1592-1597.

16. Davis, G. E. Journal of the Optical Society of America, v. 45, 1955: 572.

17. Devin, C. Survey of Thermal, Radiation, and Viscous Damping of Pulsating Air Bubbles in Water. JASA, v. 31, 1959: 1654.

18. Fox, F. E., Curley, S. R., and Larson, G. S. Phase Velocity and Absorption Measurements in Water Containing Air Bubbles. JASA, v. 27, no. 3, May 1955: 534-539.

19. Glotov, V. P., Kolobaev, P. A., and Neuimin, G. G. Investigation of the Scattering of Sound by Bubbles Generated by an Artificial Wind in Sea Water and the Statistical Distribution of Bubbles Sizes. Soviet Physics-Acoustics, v. 7, no. 4, Apr. 1962: 341-345.

20. Hansen, P. G. and Barham, E. G. Resonant Cavity Measurements of the effects of "Red Water" Plankton on the Attenuation of Underwater Sound. Limnology and Oceanography, v. 7, Jan. 1962: 8-13.

21. Hubbard, J. C. The Acoustic Resonator Interferometer: I. The Acoustic System and its Equivalent Electrical Network. Physical Review, v. 38, Sept. 1931: 1011-1019.

22. Kuttruff, H. und Wille, P. Absoluteichung verschienartiger Wasserschallwandler im Bereich von 5 bis 250 KHz. Acustica, v. 12, no. 6, 1962: 410-421.

23. Lieberman, L. Air Bubbles in Water. Journal of Applied Physics, v. 28, no. 2, Feb. 1957: 205-211.

24. Mangold, J. F. Underwater Electrostatic Transducers. Thesis, U. S. Naval Postgraduate School, 1958.

25. Schodder, G. R. and Weikhorst, F. Electrostatic Transducers with Solid Dielectric for Waterborne Sound. Acustica, v. 7, no. 1, 1957: 38-45.

26. Seki, H., Granato, A., and Truell, R. Diffraction Effects in the Ultrasonic Field of a Piston Source and their Importance in the Accurate Measurement of Attenuation. JASA, v. 28, no. 2, Mar. 1956: 230-238.

27. Truell, R. and Oates, W. Effect of Lack of Parallelism of Sample Faces on the Measurement of Ultrasonic Attenuation. JASA, v. 35, Sept. 1963: 1382.

28. Turner, W. R. Microbubble Persistence in Fresh Water. JASA, v. 33, no. 9, Sept. 1961: 1223-1233.

29. Urick, R. J. and Hoover, R. M. Backscattering of Sound from the Sea Surface. JASA v. 28, no. 6, Nov. 1956: 1038-1042.

30. Welford, W. T. Bubbles Chamber Optics. Applied Optics, v. 2, no. 10, Oct. 1963: 981-995.

31. Williams, A. O. The Piston Source at High Frequencies. JASA, v. 23, no. 1, Jan. 1951: 1-6.